Behaviour of rectangular RACFST slender columns under eccentric compression

You-Fu Yang[a,*], Feng Fu[b], Xue-Meng Bie[a]

a State Key Laboratory of Coastal and Offshore Engineering, Dalian University of Technology, Dalian 116024, China
b Department of Civil Engineering, School of Mathematics, Computer Science & Engineering, City, University of London, Northampton Square, London, UK

Abstract:

Experimental and numerical studies on the static behaviour of eccentrically compressed recycled aggregate concrete filled steel tube (RACFST) slender columns with rectangular cross-section are reported in this paper. Fifteen specimens were tested under eccentric compression. The factors considered in the experimental investigation included: 1) depth-to-width ratio (β), from 1.0 to 2.0; 2) load eccentricity ratio (m), from 0 to 0.6; 3) slenderness ratio (λ), from 20 to 40; and 4) recycled coarse aggregate (RCA) replacement ratio (r), from 0 to 100%. The experimental results show that failure of the eccentrically compressed specimens is manifested with major local buckling of the steel tube coving compression flange and part of side walls near the mid-height section and the crushing of the concrete core at the same location. The eccentrically compressed specimens generally possess stable load versus deformation curves including the initial linear and the subsequent nonlinear stages before reaching the peak load and the post-peak descending stage. In addition, when other parameters keep constant, the specimens with larger m, λ and r possess smaller bearing capacity (N_{ue}), and m has more significant effect on N_{ue} than λ and r. Numerical simulation of the eccentrically compressed rectangular RACFST slender columns is also carried out by a finite element analysis (FEA) model built in ABAQUS, and the model is verified by experimental results. The typical mechanism of rectangular RACFST slender columns under eccentric compression is further revealed by the FEA model. Finally, simplified formulae for the bearing capacity are developed, and the comparison between simplified and experimental results indicates that the simplified model is accurate in predicting the bearing capacity of rectangular RACFST slender columns.

Keywords: Recycled aggregate concrete filled steel tube (RACFST); Rectangular section; Slender columns; Experimental and numerical study; Bearing capacity.

*Corresponding author. Tel.: 86-411-8470 8510; Fax: 86-411-8467 4141.

E–mail address: youfuyang@163.com (Dr. You-Fu Yang).

1. Introduction

Recycled aggregate concrete (RAC) is one of the green building materials, as it reduces not only the disposal of waste concrete, but also the demand of natural aggregate resources by replacing them with recycled aggregates. It is believed that the rational use of RAC plays an important role in promoting sustainable development of environment, energy and economy [1-3]. Nowadays, RAC has attracted great research attention worldwide [4]; however, RAC has quite a lot of inherent defects compared with normal concrete (NC) possessing the same mix proportions [2, 3], such as lower strength and modulus of elasticity, larger shrinkage and creep, worse durability, etc. Therefore, RAC is often used as the secondary or non-structural components [3, 4]. In order to advance the structural application of the RAC, filling RAC into steel tubes is a method to ameliorate the aforementioned shortcomings of RAC [5, 6]. The research outcomes show that, recycled aggregate concrete filled steel tube (RACFST) has similar performance to traditional concrete filled steel tube (CFST), because the presence of RAC core can effectively prevent or delay the premature local buckling of steel tube under compression, and conversely, the steel tube can effectively constrain the core RAC [6-8].

As is well known, for CFST, rectangular (including square) steel tube provides a weaker constraint to its concrete core than circular steel tube under the same geometric and physical conditions. However, rectangular CFST also shows good structural performance due to the enhanced interaction between the outer tube and its concrete core [9]. In addition, rectangular CFST members have the advantages of larger moment of inertia and simpler configuration of beam to column joints than circular members [10]. Taking into account the above characteristics, rectangular CFSTs have been widely used as major structural members in building structures and bridges [9, 11].

Currently, scholars have done extensive research on the short-term static (including bond between two materials), long-term static and hysteretic behaviour of circular RACFST members [12-15]. In addition, the studies on RACFST members with square section (i.e. special case of rectangular section with depth-to-width ratio of 1.0) have also gained some attention, such as the tests reported in [6, 16-24] with recycled coarse/fine aggregate replacement ratio, steel ratio, slenderness ratio, load

eccentricity ratio and axial compression level as the main variables, and the numerical studies described in [16, 20, 21]. Nevertheless, there is few study on the structural performance of rectangular RACFST members with depth-to-width ratios greater than 1.0, especially the slender composite members. To the best of authors' knowledge, only Tam et al. [7] and Yang et al. [25] performed the experimental and finite element analysis (FEA) of the rectangular RACFST stub columns under concentric compression. In addition, based on numerical model taking into account the progressive local buckling and the initial geometric imperfections, Patel et al. [26] and Liang et al. [27] successfully simulated the structural behaviour of uniaxially and biaxially loaded high-strength thin-walled rectangular CFST slender beam-columns. These researches [7, 25-27] provide a good foundation for the study presented in this paper.

The above literature review indicates that there is limited research on the structural performance of rectangular RACFST slender columns under eccentric compression, which is a common loading case in real construction projects. Therefore, the experimental and numerical investigation in this paper are aimed to study the static behaviour of rectangular RACFST slender columns under eccentric compression. The tests of fifteen specimens with different depth-to-width ratio, load eccentricity ratio, slenderness ratio and recycled coarse aggregate (RCA) replacement ratio were performed. Finite element analysis (FEA) model of the eccentrically compressed rectangular RACFST slender columns was built, and further validated by the test results. Moreover, the FEA model was used to reveal the typical failure process and load bearing capacity of rectangular RACFST slender columns under eccentric compression. Simplified equations to predict the bearing capacity of rectangular RACFST slender columns are developed in this paper.

2. Experimental investigation

2.1 Specimens

Fifteen slender column specimens with rectangular cross-section were produced, as summarized in Table 1, where D and B are the outer depth and width of rectangular steel tube, respectively; t is the wall thickness of the steel tube; H is the height of the column; e is the load eccentricity about

major axis of cross-section, $\beta(=D/B)$ is the depth-to-width ratio; $m(=2e/D)$ is the load eccentricity ratio; $\lambda(=2\sqrt{3}H/D)$ is the slenderness ratio about major axis of cross-section; r is the recycled coarse aggregate (RCA) replacement ratio, representing the weight percentage of RCA in the whole coarse aggregate; N_{ue} is the tested bearing capacity; u_{me} is the lateral displacement at the mid-height section when N_{ue} is achieved, and N_{ufea} is the predicted bearing capacity using the FEA model.

The main parameters considered in the experiments include:

- Depth-to-width ratio (β): from 1.0 to 2.0;
- Load eccentricity ratio (m): from 0 to 0.6;
- Slenderness ratio (λ): from 20 to 40; and
- RCA replacement ratio (r): from 0 to 100%.

Rectangular steel tubes were fabricated by welding two identical cold-formed U-shaped profiles using two butt welds, and the sizes and length of the steel tubes were kept in line with the design. Both ends of the rectangular steel tubes were grinded flat, and two rectangular steel endplates with thickness of 16 mm were manufactured in the same time. Before casting the concrete from the upper opening, the lower end of the steel tubes was welded to one endplate, and after completing the concrete casting, the concrete was intentionally left slightly higher than steel tube. After two weeks of concrete curing, the tip of the concrete core was grinded to even to the steel tube with a grinding machine and the top endplate was then welded to the steel tube.

2.2 Material properties

Steel plate with the measured average wall thickness of 2.7 mm was used to produce the rectangular tubes. The properties of steel were obtained on the basis of the customary test on three tensile coupons arbitrarily cut from the steel plates. The measured average yield strength (f_{y}), tensile strength (f_{u}), elastic modulus (E_{s}), yield strain (ε_{y}), Poisson's ratio (μ_{s}) and elongation after fracture (e_{f}) respectively equal to 274.2 MPa, 424.4 MPa, 200.2 GPa, 0.00137, 0.277 and 33.9%, exhibiting the limited discrete.

Three types of concrete mix, including normal concrete (NC) with natural aggregates (i.e. $r = 0$), RAC with r of 50% (RAC1) and RAC with r of 100% (RAC2), were prepared. The RCAs were gained through crushing the waste NC from the same group reinforced concrete members by a jaw crusher, and the cube compressive strength of the original concrete was about 50 MPa. The particle size of RCA ranged from 5 to 25 mm, and the particle gradation, the crushing index, the water absorption ratio, the needle-like particle content, the toughness and the mud content of RCA were all in compliance with the related provisions stipulated in the Chinese standard [28]. The natural coarse aggregates (NCAs) were carbonaceous stone with the same particle size range as the RCAs. The rest of the materials used while producing the concrete included: grade 42.5 Portland cement, natural yellow sand (medium sand), Sika polycarboxylate water reducing agent (WRA) and tap water. These three types of concrete had the same mix proportions for the purpose of comparative studies, as listed in Table 2. The concrete properties, including the cubic compressive strength (f_{cu}), the modulus of elasticity (E_{c}) and the slump height, were respectively obtained by the cube (side lengths of 150 mm) compression test, the prism (side lengths of 150 mm×150 mm×300 mm) compression test and the slump test, and the measured mean values are also included in Table 2, in which $f_{\mathrm{cu,28}}$ and $f_{\mathrm{cu,t}}$ are the average cubic compressive strength at 28-day and during the test day. It can be observed from Table 2 that, the cubic compressive strength, the modulus of elasticity and the slump height of RAC are smaller than those of the reference NC, and RAC with a larger r possesses a worse feature. This is attributed to the fact that, the RCA is rougher than the NCA since the accompanied old mortar with a larger water absorption and a lower strength is attached to the outside of the former [2, 3].

2.3 Tests under eccentric compression

The tests of the specimens under eccentric compression were performed on a 5,000 kN capacity testing machine, and the test set-up and instrumentation are shown in Fig. 1. During the tests, both the upper and lower endplates of the specimen were compressed with the aid of knife hinges acting on the loading plate to replicate the boundary conditions of the hinged ends, and the applied loads were recorded by a load cell placed between the connecting plate of the knife hinge and the top platen

of the testing machine. The equal eccentricity at both ends of the specimen was controlled by the vertical distance between the V-shaped grooves on the loading plate and the cross-sectional centroid. To guarantee sufficient rotation capacity of the endplates, the depth of the V-shaped grooves was made smaller than the height of the knife hinge, and under the same plane the width of the V-shaped grooves was larger than that of the knife hinge. A protecting steel frame was specially fabricated to ensure the safety of the data acquisition equipment during the loading and unloading phases. To track the strain reading on the outer surface of the steel tube at the mid-height section, strain gauges (SGs) were attached in longitudinal and transverse direction at 4 points on the symmetric axis, and SGs were also placed in longitudinal direction at another 4 points close to the tube corner. In addition, 4 displacement transducers (DTs) were set on the bottom platen of the testing machine to record the axial displacements, and another 3 evenly spaced DTs were set along the height of the specimen to capture the lateral displacements.

The tests were carried out using both load-control and displacement-control methods. Before achieving the peak load, the load steps of one tenth to one fifteenth of the estimated bearing capacity were adopted with the loading rate of 0.5 kN/s, and each step was maintained for about 2 minutes. After the peak load reached, the tests were controlled by the axial displacement of the specimen, and the rate of displacement increase was 0.2 mm/min. When the load borne by the specimen dropped to 60% of the peak load, or the lateral displacement at mid-height section was greater than 2% of the specimen height, the tests were ceased.

2.4 Test results and analysis

Similar to those reported in the previous tests [16, 17, 22-24], three stages can be identified for the tested specimens, and good bearing capacity and deformability were observed during the tests. In the first stage, the load and displacement/strain raised approximately linearly and the deformation of the steel tube was not obvious. In the second stage till the peak load, the load and displacement/strain increased nonlinearly with a faster displacement/strain increase, and the compression flange of the steel tube near the mid-height of the column generally began to buckle with the sound of concrete

crushing. In the final stage after the peak load, the load borne by the column decreased rapidly with an increase of the displacement, and the deformation of the buckled steel tube further increased together with the subsequent compressive buckling of the tube side walls.

Fig. 2 demonstrates the failure pattern of the specimens after tests, where the buckled positions of the steel tube are indicated by the arrows. It can be seen that, in general, the local buckling of the steel tube of concentrically compressed columns only occurs along the side walls. This is due to the fact that the tube side walls with a larger width-to-thickness ratio provide a weaker constraint to the concrete core than their neighboring tube flanges. For the eccentrically compressed columns, in general, there is one major local buckling along the compression flange near the mid-height section and several subsequent slight local buckling at the tube side walls along the height, except for the two specimens with a larger slenderness ratio (i.e. B0.3-40-RAC1 and C0.3-36-RAC1), having only one major local buckling of the steel tube at the mid-height section coving compression flange and part of side walls, due to a larger second-order effect under axial compression. However, not all the major local buckling of the steel tube is located near the mid-height of the specimens, which is caused by the material defects variation in a tube. It should be noted that, the local buckling of the steel tube of four eccentrically compressed specimens (i.e. A0.3-30-RAC1, B0.6-30-RAC1, C0.6-30-RAC1 and C0.3-30-RAC2) only happened at one end, which may be induced by the concentration of material defects. Overall, when other parameters keep constant, the peak outward deformation of the major compressive buckling of the steel tube increases with an increase of β, m and λ, and r has a moderate effect, whilst the number of the subsequent local buckling of the tube side walls decreases with a decrease of m and an increase of λ and r, and β has no evident influence.

Typical failure pattern of the concrete core is indicated in Fig. 3. It can be seen that, there is no apparent damage to the concrete core of the concentrically compressed specimens as the steel tube only slightly buckles along the side walls. Moreover, the concrete core of the eccentrically compressed specimens is generally crushed at the major local buckling position of the steel tube, which is similar to the observed phenomena in the previous tests [16, 17, 22, 23], and there is also no

obvious destruction to the concrete core at the subsequent buckling position of the tube side walls. This shows that, in the stage after reaching the peak load, the discrepancy in compressive and flexural deformation induced by the difference in compressive and flexural stiffness between steel tube and concrete core only leads to the subsequent slight local buckling of the tube side walls with a larger D/t ratio, and no new damage to the concrete core happens.

The effect of parameters on the measured load (N) versus axial displacement (δ) relationship of the specimens is shown in Fig. 4, and the axial displacements equal to the mean of the results measured by the four DTs. It can be seen that, the $N-\delta$ curves all include the initial linear and the subsequent nonlinear stage before reaching the peak load and the post-peak descending stage. Generally, the slope of the linear stage of the $N-\delta$ curve decreases with an increase of m, λ and r and increases with an increase of β, due to the increased second-order effect, the decreased E_{c} and the increased area of concrete core. The peak load on the $N-\delta$ curve is defined as the bearing capacity (N_{ue}) of the specimens, which are listed in Table 1.

It was observed from the tests that, except for 2 concentrically compressed specimens and 4 eccentrically compressed specimens possessing local failure at one end, the lateral displacements (u) shape along the height of the eccentrically compressed specimens generally followed half-sine wave curve, as typically demonstrated in Fig. 5, where the solid lines represent the measured results, the dashed lines are the half-sine wave curve with the lateral displacements at the mid-height section equal to the tested values, h is the distance from the bottom end of the specimen, and n (=N/N_{ue}) is the load ratio and negative value of n represents the post-peak phase.

The relationship between load (N) and lateral displacement at the mid-height section (u_{m}) of the specimens changes with the variation of experimental parameters, as demonstrated in Fig. 6. It can be seen that, in general, the initial slope of $N-u_{\mathrm{m}}$ curve decreases, the $N-u_{\mathrm{m}}$ curve enters the nonlinear stage earlier and the load decline rate after the peak reduces with an increase of m, λ and r. This can be attributed to the increased second-order effect with an increase of m and λ, and the decreased E_{c} with increasing r. Moreover, with increasing β, the initial slope of $N-u_{\mathrm{m}}$ curve

increases, the $N-u_{\mathrm{m}}$ curve enters the nonlinear stage earlier and the load decline rate after the peak reduces, due to the increased cross-sectional area of RACFST, the concrete core under tension and the steel tube in tension after the peak load, respectively.

Fig. 7 shows the load (N) versus strain (ε) relationship at the mid-height section of two typical specimens, where the strain at the symmetry points (2 and 4) is averaged, tensile and compressive strains are respectively regarded as positive and negative, and the capital letters 'L' and 'T' in the brackets represent the longitudinal and transverse strain, respectively. It can be seen that, the $N-\varepsilon$ curve has the similar development process as the $N-\delta(u_{\mathrm{m}})$ curve, and it also contains linear and nonlinear phases before the peak load and the post-peak falling phase. Generally, along the side walls of the steel tube, the strain at the corners develops faster than that at the symmetric axis, indicating that the confinement of rectangular steel tube to its concrete core at the corners is stronger than that at the middle of the section, and the compressive strain develops faster than the tensile strain under eccentric compression. Generally, the development of the transverse strains is similar to that of the longitudinal strains, but the signs of them are opposite due to the Poisson effect. For the specimens with a relatively small m, the longitudinal strains at point 3 on the centroid axis are always maintained in compression. Moreover, the specimens with a larger β have a higher strain due to the increased distance from the outermost tube flange to the centroid axis. Based on the detailed analysis of the measured strains, it is found that, the longitudinal strain of the steel tube is approximately linearly distributed along the section depth before reaching the bearing capacity, which means that the mid-height section of the rectangular RACFST slender columns under eccentric compression basically conforms to the 'plane sections remain plane' assumption.

The effect of parameters on load (N) versus longitudinal strain at point 1 ($\varepsilon_{l,1}$) curves is demonstrated in Fig. 8. It can be observed that, $\varepsilon_{l,1}$ of all specimens is far greater than ε_{y} while the peak load achieved, indicating that the ultimate capacity of the tube compression flange can be fully utilized. Furthermore, the impact of each parameter on the development of the rising stage of the $N-\varepsilon_{l,1}$ curve before the peak load is basically the same as that of the $N-\delta(u_{\mathrm{m}})$ curve. However,

the influence of each parameter on the development of the post-peak descending stage of the $N-\varepsilon_{l,1}$ curve is more ambiguous. This is mainly due to the fact that, the major local buckling portion of the steel tube of several specimens does not occur at point 1, resulting in constant or even reduce of strain with a decrease of loads.

Fig. 9 shows the influence of parameters on the measured bearing capacity (N_{ue}). It can be seen that, N_{ue} of the specimens with the same B value increases with increasing β due to the increased cross-sectional area, and N_{ue} of the specimens with β of 1.5 and 2.0 is 1.3 times and 1.67 times of that with β of 1.0 (square one). While keeping other parameters constant, N_{ue} of the specimens decreases with an increase of m, λ and r due to the increased second-order effect and the decreased concrete strength. Overall, m has most obvious influence on N_{ue}, followed by λ, indicating that the load eccentricity and the second-order effect are the main factors determining the bearing capacity of a rectangular RACFST slender column. The specimens with m of 0.3 and 0.6 respectively result in 26.6~50.6% ($\beta=1.5$) and 11.2~36.4% ($\beta=2.0$) lower N_{ue} than those with m of zero, and N_{ue} of the specimens with λ of 30 and 40/36 is 4.1~12.5% ($\beta=1.5$) and 7.9~8.4% ($\beta=2.0$) lower than that of the specimens with λ of 20, respectively. However, r has a relatively small effect on N_{ue} as the confinement of the steel tube alleviates the degree of the decrease of the core RAC strength with increasing r, which is similar to the findings in previous studies [7, 19]. When r is increased from zero to 50% and 100%, 1.0~2.8% ($\beta=1.5$) and 3.9~10.9% ($\beta=2.0$) lower N_{ue} is respectively produced.

The effect of parameters on the lateral displacement at the mid-height while achieving N_{ue} (u_{me}) is demonstrated in Fig. 10. It is shown that, while keeping the remaining parameters constant, u_{me} generally increases with an increase of β, m and λ mainly due again to the increased second-order effect. The specimens with β of 1.5 and 2.0 respectively possess 56% and 98% larger u_{me} than the corresponding specimen with β of 1.0, and u_{me} of the specimens with λ of 30 and 40/36 are 2.7~3.7 times ($\beta=1.5$) and 2.5~3.1 times ($\beta=2.0$) of that of the specimens with $\lambda=20$, respectively. However, the concentrically compressed specimens have a very small u_{me}, which is

about 13% ($\beta = 1.5$) and 8% ($\beta = 2.0$) of that of the corresponding eccentrically compressed specimens. Moreover, take $r = 50\%$ as the boundary, u_{me} increases first and then decreases with increasing r. The increased u_{me} is attributed to the decreased E_{c} when $r \leq 50\%$; however, more defects in the RAC may cause premature destruction of the specimens when $r = 100\%$. Generally, when r is increased from zero to 50% and 100%, about 4.5% larger and 2.0% lower u_{me} is produced.

The impact of parameters on $\varepsilon_{\mathrm{ue},l}/\varepsilon_{\mathrm{y}}$ is shown in Fig. 11, where $\varepsilon_{\mathrm{ue},l}$ is the longitudinal strain recorded at each measuring point while reaching N_{ue}. It is shown that, for the concentrically compressed specimens, the compressive strains of the measuring points are almost approximative regardless of β value. This is generally consistent with the failure characteristics of the specimens, i.e. there is no obvious lateral displacement occurred at the mid-height section (see Fig. 2(b)). For the eccentrically compressed specimens, the mid-height section of the column has both compressive and tensile portion, and the cross-sectional centroid axis (point 3) is in the compressive portion while reaching N_{ue}. The strain of the compression flange of the steel tube is fully developed, and $\varepsilon_{\mathrm{ue},l}$ at the corner (point 2) is larger than that at the symmetry axis (point 1). The calculated results show that $\varepsilon_{\mathrm{ue},l}$ of the compression flange of the steel tube is about 2~6 times of ε_{y}. The longitudinal strain of the tension flange of the steel tube is not fully developed as the cross-section at the mid-height is mainly under compression, and the strain difference between the corner (point 4) and the symmetry axis (point 5) is not obvious. At the same time, there are only a few cases in which $\varepsilon_{\mathrm{ue},l}$ of the tube tension flange is greater than ε_{y}.

3. Numerical simulation

3.1. Finite element analysis (FEA) model

In order to simulate the behaviour of the eccentrically compressed rectangular RACFST slender columns, a three-dimensional nonlinear finite element analysis (FEA) model was established using ABAQUS software [29].

The adopted constitutive model for the steel tube and the concrete core consisted of both elastic

and plastic stages of the material. The elastic modulus and the Poisson's ratio of steel were obtained from tensile coupon tests, and those of concrete were set to be $4730\sqrt{f_c'}$ [30] and 0.2 [25] respectively, where f_c' is the cylinder compressive strength of concrete converted from $f_{\mathrm{cu,t}}$ according to the provisions in [31]. In simulating the plasticity of steel a classical metal plasticity model in ABAQUS [29] was used, with the true stress versus plastic strain relationship derived from the nominal one for the cold-formed steel suggested in [32], and the inelastic behaviour of concrete core was modelled by the damaged plasticity model in ABAQUS [29], with the yield and failure surface controlled by the equivalent plastic strain and the stiffness degradation characterized by the damage variables. To obtain the compressive stress-inelastic strain data of the RAC core in rectangular steel tube, the nominal compressive stress-strain relationship in [25] was adopted, and thus the influence of the confinement of rectangular steel tube to the RAC core on the post-peak phase of the compressive stress-strain relationship was considered. Moreover, the fracture energy cracking criterion was utilized to specify the tension stiffening of the core RAC.

Four-node reduced integration shell elements (S4R) were employed to model the rectangular steel tube, and eight-node reduced integration linear brick elements (C3D8R) were adopted to simulate the concrete core and two endplates. The final mesh density was determined based on the difference of the simulated bearing capacity between two adjacent meshes within 1%. For the main contact between the inner surface of the tube and the concrete core, the hard contact and the Coulomb friction with a friction coefficient of 0.6 [25] were defined in the normal direction and the tangential directions, respectively. In addition, the contact (welding) between the tube ends and the endplates was defined as the shell-brick coupling constraints, and the normal contact between the concrete core and the end plate was set as hard contact while ignoring the tangential contact.

The FEA model of rectangular RACFST slender columns under eccentric compression is demonstrated in Fig. 12. To replicate the function of the knife hinge (see Fig. 1), a loading line was set on each of the upper and lower endplates, and the perpendicular distance from the loading line to the cross-sectional centroid axis was equal to the load eccentricity (e) in the tests. Moreover, a load

eccentricity of $H/1000$ was employed to consider the effect of the initial geometric imperfection of the columns [21, 26, 27]. Boundary conditions of the FEA model are shown in Fig. 12. In the initial analysis step, all displacements of the loading line on the lower endplate were restricted, and the translations in X and Y directions of the loading line on the upper endplate were restricted. In the follow-up analysis step, an axial displacement (δ) of 50 mm along the Z direction was exerted to the loading line on the upper endplate of the column.

3.2. Verification of the FEA model

The predicted typical failure pattern of typical specimens together with the Mises stress of the steel tube are shown in Fig. 13. It can be found from the comparison between Fig. 13 and Fig. 2 that, except for the four aforementioned eccentrically compressed specimens with one end buckling of the steel tube, the predicted results generally represent the behaviour of the specimens, i.e. the local buckling of the steel tube of the concentrically compressed columns mainly occurs near the ends, while the local buckling of the steel tube (including compression flange and part of side walls) of the eccentrically compressed columns is mainly concentrated near the mid-height section. However, there is a certain difference between the simulated and observed buckling position of the tube, because the steel tube and its concrete core in the FEA model are simulated using idealized materials model, while the materials of the test specimens have randomly distributed defects. Moreover, the Mises stresses of the steel tube of the eccentrically compressed columns is generally attenuated from the mid-height section to both ends, indicating that the final failure of the rectangular RACFST slender columns under eccentric compression is controlled by the destruction of the mid-height section. Fig. 14 demonstrates the predicted typical failure pattern together with the logarithmic strain along the vertical direction (LE33) of the concrete core in the steel tube. According to the contrast between Fig. 14 and Fig. 3, it can be discovered that, the concrete destruction of the eccentrically compressed column is generally concentrated on 1~2 positions near the mid-height section, and the compressive LE33 at the major local buckling position of the tube compression flange is the largest. In addition, the concrete core of the concentrically compressed column also shows local failure near the ends.

The comparison between the predicted and measured $N-u_{\mathrm{m}}$ curves is depicted in Fig. 6. It can be seen that, both curves have the similar trend although the simulated initial slope, the bearing capacity and the descending stage after the peak are slightly different from the measured results; however, the four aforementioned eccentrically compressed specimens with one end failure show a larger difference. The divergence between the predicted and measured $N-u_{\mathrm{m}}$ curves may because of the existence of initial defects, such as the difference between the properties of the materials in the composite specimens and those measured by the concrete blocks and steel coupons, initial cracks in the concrete core, possible gap between steel tube and core concrete, and the difference between the simulated and observed steel tube buckling position and/or range after the peak load. Fig. 8 shows the typical comparison between the simulated and recorded $N-\varepsilon_{l,1}$ curves of the specimens. It can be seen that, before reaching the peak load, the predicted $N-\varepsilon_{l,1}$ curves generally agree well with the recorded ones. However, after achieving the peak load, the simulated curves are unloaded at a constant slope as the strain increases, showing a significant difference from the measured ones. This can be explained by that, point 1 in the FEA model is exactly the buckling position of the tube compression flange, whilst point 1 on the specimens is generally not the exact position where the steel tube is buckled under compression. The predicted bearing capacities (N_{ufea}) by the FEA model are compared with N_{ue} in Fig. 15 and Table 1. Analysis on the data indicates that, the mean and standard deviation of $N_{\mathrm{ufea}}/N_{\mathrm{ue}}$ are equal to 0.989 and 0.044, respectively, and the discrepancy between N_{ufea} and N_{ue} is within 10%. This demonstrates that the predicted bearing capacities of rectangular RACFST slender columns under eccentric compression using the FEA model generally accord well with the measured results.

Although there are divergences between the predicted load (N) versus deformation (u_{m} and $\varepsilon_{l,1}$) curves and the measured results, the predicted failure patterns, bearing capacities as well as development trend of lateral displacements and strains at the mid-height section are generally in good agrement with the recorded results. Therefore, it can be considered that the FEA model built in this study is capable of well simulating the performance of rectangular RACFST slender columns under

eccentric compression.

3.3. Mechanism analysis using the FEA model

Based on the validated FEA model, the investigation into the typical mechanism of rectangular RACFST slender columns under eccentric compression was carried out. The geometric and physical conditions of the benchmark composite member included: $D \times B = 480 \times 320$ mm ($\beta = 1.5$), $m = 0.5$, $\lambda = 40$, $r = 50\%$, steel ratio $\alpha = 0.1$, $f_y = 355$ MPa, and $f_c' = 50$ MPa, where α is the ratio of cross-sectional area of steel to that of concrete core. In addition, to ensure comparability, the cross-sectional area of the composite member was kept constant when β was varied.

The simulated results indicated that, except for the composite columns with a relatively small m and λ, the concrete core at the mid-height section of the column had both tension and compression zone, and when other parameters kept constant the sectional height of the tension zone increased with an increase of β, m, λ, f_y and f_c' and a decrease of α, whilst r had a moderate impact. The highest longitudinal stress of the core RAC higher than f_c' appeared at the corner of the compression zone due to a stronger constraint from the steel tube. Furthermore, the maximum longitudinal stress of the core RAC at the corner lessened with a growing of β, λ and r and a lowering of m, α, f_y and f_c'. The influence of typical parameters on longitudinal stress of core RAC (S33) at the mid-height section of the column while achieving the bearing capacity is shown in Fig. 16.

Typical variation of interaction stress between the steel tube and the concrete core (p) at the mid-height section of the column with the increase of u_m is demonstrated in Fig. 17, where the triangles represent the moment when the column reaches its bearing capacity. It can be seen that, under the same u_m, p at the corners of the section (points b and d) are significantly higher than those at other points, and before reaching the bearing capacity the difference of p between points b and d is not apparent. However, after the bearing capacity is achieved p of point d gradually exceeds that of point b owing to the local buckling of steel tube near point b. The interaction stress (p) at the mid-point of the tube tension flange (point f) is quite small, and p at points a and c are close to zero due mainly to the separation between the steel tube and the concrete core caused by the local buckling of

the steel tube. These indicate that the interaction between the steel tube and the concrete core is mainly distributed at the corners of the section. The effect of key parameters on $p-u_{\mathrm{m}}$ relationship at point b is presented in Fig. 18. It is shown that, under the same u_{m}, p decreases with an increase of β, m and λ due to the increased second-order effect. However, r has a moderate effect on the development of $p-u_{\mathrm{m}}$ relationship.

4. Simplified formulae

To obtain the simplified formulae for the bearing capacity prediction of rectangular RACFST slender columns under eccentric compression, parametric analysis on the axial load ratio (N/N_0) versus the moment ratio (M/M_{u}) relationship was performed using the FEA model, where N and M are the applied axial compressive load and moment respectively, and M equals to $N\cdot e$; N_0 and M_{u} are the cross-sectional strength and moment capacity, respectively. The simulation results indicated that, for the N/N_0 versus M/M_{u} relationship, the influence of α, f_{y} and f_{c}' could be unified as the effect of the confinement factor (ξ_{r}) [12]. The impact of β, r, ξ_{r} and λ on the N/N_0 versus M/M_{u} relationship is plotted in Fig. 19 by the solid lines. It can be seen that, while keeping other parameters constant, the bearing capacity of the column decrease with an increase of r and λ and a decrease of ξ_{r}, and β generally has a moderate effect on the bearing capacity of the column.

A large number of numerical simulations and further date analysis showed that the simplified N/N_0 versus M/M_{u} correlation equations for square RACFST slender columns under eccentric compression in [12] were also suitable for rectangular ones, and the formulae are as follows:

$$\begin{cases} \dfrac{N}{\varphi N_0}+\dfrac{a}{d}\dfrac{M}{M_{\mathrm{u}}}=1 & \left(\dfrac{N}{N_0}\geq 2\varphi^3\eta_0\right) \\ -b\left(\dfrac{N}{N_0}\right)^2-c\dfrac{N}{N_0}+\dfrac{1}{d}\dfrac{M}{M_{\mathrm{u}}}=1 & \left(\dfrac{N}{N_0}<2\varphi^3\eta_0\right) \end{cases} \tag{1}$$

where, φ is the stability factor, a, b, c and η_0 are the intermediate variables, and d is the factor considering the second-order effect. The specific simplified formulae for N_0 and M_{u} are detailed in [12].

The simplified N/N_0 versus M/M_{u} relationship indicated by the dashed lines are also presented

in Fig. 19. It can be seen that both the simplified and FEA curves have the same trend and similar predictions. Fig. 20 demonstrates the effect of β and r on $N_{\mathrm{us}}/N_{\mathrm{ue}}$ of rectangular RACFST slender columns under eccentric compression, where N_{us} is the simplified bearing capacity, and the effective test data in this study and those from the literatures (58 in total) are covered in the comparison. It can be found that a suitable fitness between the simplified and experimental bearing capacities is attained, considering that the mean and standard deviation of $N_{\mathrm{us}}/N_{\mathrm{ue}}$ equal to 0.907 and 0.111, respectively. The application scope of the simplified equations is: $\beta = 1.0\sim2.0$, $r = 0\sim100\%$, $\alpha = 0.05\sim0.2$, $f_{\mathrm{y}} = 200\sim500$ MPa, and $f_{\mathrm{c}}' = 25\sim65$ MPa.

5. Conclusions

Based on the experimental and numerical studies on the eccentrically compressed rectangular RACFST slender columns, the following conclusions can be drawn:

(1) After completing the tests, the eccentrically compressed rectangular RACFST slender columns generally have local buckling observed in compression flange and part of side walls of the steel tube near the mid-height section, and the columns with a larger β, m and λ possess a larger peak outward deformation of the steel tube at the major local buckling portion. Generally, the concrete core is crushed at the major local buckling portion of the steel tube.

(2) The load (N) versus deformation (δ, u_{m} and ε) curve of rectangular RACFST slender column specimens under eccentric compression consists of initial linear and the subsequent nonlinear stages before reaching the peak load and the post-peak descending stage. Generally, the initial slope of the load versus deformation curve decreases with an increase of m, λ and r and a decrease of β.

(3) When other parameters keep constant, the columns with a larger m, λ and r tend to have a lower N_{ue}, while those having a larger β end up with a higher N_{ue}. Overall, compared with the smallest β, m, λ and r values (1.0, 0, 20 and 0), the columns with a larger β, m, λ and r result in 30~67% higher, 11.2~50.6% lower, 4.1~12.5% lower and 1.0~10.9% lower N_{ue}, respectively.

(4) The simulated responses of rectangular RACFST slender columns under eccentric compression using the established FEA model generally agree well with the experimental observations. Parametric

analysis results reveal the impact of key factors on the mechanism of the eccentrically compressed rectangular RACFST slender columns.

(5) The simplified equations for the axial load ratio versus moment ratio of rectangular RACFST slender columns under eccentric compression are suggested, from which the calculated bearing capacities are in good agreement with the experimental results.

Declaration of Competing Interest

The authors declare that they have no known competing financial interests or personal relationships that could have appeared to influence the work reported in this paper.

Acknowledgements

The studies in this paper are financially supported by the National Natural Science Foundation of China (Grant No. 51678105). The financial support is gratefully acknowledged.

References:

[1] J. Nobre, M. Bravo, J. de Brito, G. Duarte, Durability performance of dry-mix shotcrete produced with coarse recycled concrete aggregates, Journal of Building Engineering 29 (2020) 101135.

[2] T. C. Hansen, Recycling of Demolished Concrete and Masonry, Report of RILEM TC 37-DRC on Demolition and Reuse of Concrete, E&FN Spon, London, UK, 1992.

[3] E. Vázquez, Progress of Recycling in the Built Environment, Final Report of the RILEM Technical Committee 217-PRE, Springer, Heidelberg, Germany, 2013.

[4] V. W. Y. Tam, M. Soomro, A. C. J. Evangelista, A review of recycled aggregate in concrete applications (2000-2017), Construction and Building Materials 172 (2018) 272-292.

[5] K. Konno, Y. Sato, Y. Kakuta, M. Ohira, Property of recycled concrete column encased by steel tube subjected to axial compression, Transactions of the Japan Concrete Institute 19(2) (1997) 231-238.

[6] Y. F. Yang, L. H. Han, Compressive and flexural behaviour of recycled aggregate concrete filled steel tubes (RACFST) under short-term loadings, Steel and Composite Structures 6(3) (2006) 257-284.

[7] V. W. Y. Tam, Z. B. Wang, Z. Tao, Behaviour of recycled aggregate concrete filled stainless steel stub columns, Materials and Structures 47(1-2) (2014) 293-310.

[8] W. Li, J. Xiao, C. Shi, C. S. Poon. Structural behaviour of composite members with recycled aggregate concrete-an overview, Advances in Structural Engineering 18(6) (2015) 919-938.

[9] L. H. Han, W. Li, R. Bjorhovde, Developments and advanced applications of concrete-filled steel tubular (CFST) structures: Members, Journal of Constructional Steel Research 100 (2014) 211-228.

[10] Y. Du, Z. Chen, J. Y. R. Liew, M. X. Xiong, Rectangular concrete-filled steel tubular beam-columns using high-strength steel: Experiments and design, Journal of Constructional Steel Research 131 (2017) 1-18.

[11] X. L. Zhao, L. H. Han, H. Lu, Concrete-Filled Tubular Members and Connections, Taylor and Francis, Oxford, UK, 2010.

[12] Y. F. Yang, C. Hou, Behaviour and design calculations of recycled aggregate concrete filled steel tube (RACFST) members, Magazine of Concrete Research 67(11) (2015) 611-620.

[13] J. Chen, Y. Wang, C. W. Roeder, J. Ma, Behavior of normal-strength recycled aggregate concrete filled steel tubes under combined loading, Engineering Structures 130 (2017) 23-40.

[14] W. Q. Lyu, L. H. Han, Investigation on bond strength between recycled aggregate concrete (RAC) and steel tube in RAC-filled steel tubes, Journal of Constructional Steel Research 155 (2019) 438-459.

[15] V. W. Y. Tam, J. Xiao, S. Liu, Z. Chen, Behaviors of recycled aggregate concrete-filled steel tubular columns under eccentric loadings, Frontiers of Structural and Civil Engineering 13(3) (2019) 628-639.

[16] Y. F. Yang, L. H. Han. Experimental behaviour of recycled aggregate concrete filled steel tubular columns, Journal of Constructional Steel Research 62(12) (2006) 1310-1324.

[17] Z. Chen, S. Zheng, Q. Li, J. Xue, B. Chen, Experimental study on behavior of recycled aggregate concrete filled square steel tubular long columns under eccentric compression loading, Journal of Building Structures 33(9) (2012) 21-29. (in Chinese)

[18] Z. Chen, C. Jing, J. Xu, X. Zhang, Seismic performance of recycled concrete-filled square steel tube columns, Earthquake Engineering and Engineering Vibration 16(1) (2017) 119-130.

[19] Y. F. Yang, G. L. Ma. Experimental behaviour of recycled aggregate concrete filled stainless steel tube stub columns and beams, Thin-Walled Structures 66 (2013) 62-75.

[20] Y. F. Yang, Z. C. Zhang, F. Fu, Experimental and numerical study on square RACFST members under lateral impact loading, Journal of Constructional Steel Research 111 (2015) 43-56.

[21] Y. F. Yang, L. Zhang, X. Dai, Performance of recycled aggregate concrete filled square steel tubular columns exposed to fire, Advances in Structural Engineering 20(9) (2017) 1340-1356.

[22] N. Hu, X. Du, P. Liu, Z. Niu, Experimental study on mechanical behavior of recycled aggregate concrete-filled square steel tubular long columns under eccentric compression loading, Journal of Building Structures 37(Suppl. 2) (2016) 36-42. (in Chinese)

[23] Y. Xu, Y. Yao, Z. Zhang, D. Chen, Experimental research on mechanical behavior of recycled aggregate concrete filled square steel tubular long columns under eccentric compression loading,

Building Structure 46(9) (2016) 69-74. (in Chinese)

[24] X. Yu, C. Wang, B. Liu, Q. Hu, J. Chen, Experimental study of the behavior of recycled aggregate concrete filled square steel tubular long columns under eccentric compression, Journal of Hefei University of Technology 40(8) (2017) 1110-1116. (in Chinese)

[25] Y. F. Yang, C. Hou, M. Liu, Tests and numerical simulation of rectangular RACFST stub columns under concentric compression, Structures 27 (2020) 396-410.

[26] V. I. Patel, Q. Q. Liang, M. N. S. Hadi, High strength thin-walled rectangular concrete-filled steel tubular slender beam-columns, Part I: Modeling, Journal of Constructional Steel Research 70 (2012) 377-384.

[27] Q. Q. Liang, V. I. Patel, M. N. S. Hadi, Biaxially loaded high-strength concrete-filled steel tubular slender beam-columns, Part I: Multiscale simulation, Journal of Constructional Steel Research 75 (2012) 64-71.

[28] GB/T 25177, Recycled Coarse Aggregate for Concrete, Standards Press of China, Beijing, 2010. (in Chinese)

[29] Simulia, ABAQUS 6.14 Analysis User's Manual, Dassault Systemes Simulia Corp., Providence, RI, USA, 2014.

[30] ACI Committee 318, ACI 318-19 — Building Code Requirements for Structural Concrete and Commentary, American Concrete Institute, Farmington Hills, Michigan, USA, 2019.

[31] CEN, EN 1992-1-1. Eurocode 2: Design of Concrete Structures—Part 1-1: General Rules and Rules for Buildings, 2004.

[32] N. Abdel-Rahman, K. S. Sivakumaran, Material properties models for analysis of cold-formed steel members, Journal of Structural Engineering ASCE 123(9) (1997) 1135-1143.

- Tests on the behaviour of rectangular RACFST slender columns under eccentric compression
- A three-dimensional FEA model that can well simulate the performance of eccentrically compressed rectangular RACFST slender columns
- Simplified formulae capable of well predicting the bearing capacity of rectangular RACFST slender columns

Behaviour of rectangular RACFST slender columns under eccentric compression

You-Fu Yang[a,*], Feng Fu[b], Xue-Meng Bie[a]

a State Key Laboratory of Coastal and Offshore Engineering, Dalian University of Technology, Dalian 116024, China
b Department of Civil Engineering, School of Mathematics, Computer Science & Engineering, City, University of London, Northampton Square, London, UK

Abstract:

Experimental and numerical studies on the static behaviour of eccentrically compressed recycled aggregate concrete filled steel tube (RACFST) slender columns with rectangular cross-section are reported in this paper. Fifteen specimens were tested under eccentric compression. The factors considered in the experimental investigation included: 1) depth-to-width ratio (β), from 1.0 to 2.0; 2) load eccentricity ratio (m), from 0 to 0.6; 3) slenderness ratio (λ), from 20 to 40; and 4) recycled coarse aggregate (RCA) replacement ratio (r), from 0 to 100%. The experimental results show that failure of the eccentrically compressed specimens is manifested with major local buckling of the steel tube coving compression flange and part of side walls near the mid-height section and the crushing of the concrete core at the same location. The eccentrically compressed specimens generally possess stable load versus deformation curves including the initial linear and the subsequent nonlinear stages before reaching the peak load and the post-peak descending stage. In addition, when other parameters keep constant, the specimens with larger m, λ and r possess smaller bearing capacity (N_{ue}), and m has more significant effect on N_{ue} than λ and r. Numerical simulation of the eccentrically compressed rectangular RACFST slender columns is also carried out by a finite element analysis (FEA) model built in ABAQUS, and the model is verified by experimental results. The typical mechanism of rectangular RACFST slender columns under eccentric compression is further revealed by the FEA model. Finally, simplified formulae for the bearing capacity are developed, and the comparison between simplified and experimental results indicates that the simplified model is accurate in predicting the bearing capacity of rectangular RACFST slender columns.

Keywords: Recycled aggregate concrete filled steel tube (RACFST); Rectangular section; Slender columns; Experimental and numerical study; Bearing capacity.

*Corresponding author. Tel.: 86-411-8470 8510; Fax: 86-411-8467 4141.

E–mail address: youfuyang@163.com (Dr. You-Fu Yang).

1. Introduction

Recycled aggregate concrete (RAC) is one of the green building materials, as it reduces not only the disposal of waste concrete, but also the demand of natural aggregate resources by replacing them with recycled aggregates. It is believed that the rational use of RAC plays an important role in promoting sustainable development of environment, energy and economy [1-3]. Nowadays, RAC has attracted great research attention worldwide [4]; however, RAC has quite a lot of inherent defects compared with normal concrete (NC) possessing the same mix proportions [2, 3], such as lower strength and modulus of elasticity, larger shrinkage and creep, worse durability, etc. Therefore, RAC is often used as the secondary or non-structural components [3, 4]. In order to advance the structural application of the RAC, filling RAC into steel tubes is a method to ameliorate the aforementioned shortcomings of RAC [5, 6]. The research outcomes show that, recycled aggregate concrete filled steel tube (RACFST) has similar performance to traditional concrete filled steel tube (CFST), because the presence of RAC core can effectively prevent or delay the premature local buckling of steel tube under compression, and conversely, the steel tube can effectively constrain the core RAC [6-8].

As is well known, for CFST, rectangular (including square) steel tube provides a weaker constraint to its concrete core than circular steel tube under the same geometric and physical conditions. However, rectangular CFST also shows good structural performance due to the enhanced interaction between the outer tube and its concrete core [9]. In addition, rectangular CFST members have the advantages of larger moment of inertia and simpler configuration of beam to column joints than circular members [10]. Taking into account the above characteristics, rectangular CFSTs have been widely used as major structural members in building structures and bridges [9, 11].

Currently, scholars have done extensive research on the short-term static (including bond between two materials), long-term static and hysteretic behaviour of circular RACFST members [12-15]. In addition, the studies on RACFST members with square section (i.e. special case of rectangular section with depth-to-width ratio of 1.0) have also gained some attention, such as the tests reported in [6, 16-24] with recycled coarse/fine aggregate replacement ratio, steel ratio, slenderness ratio, load

eccentricity ratio and axial compression level as the main variables, and the numerical studies described in [16, 20, 21]. Nevertheless, there is few study on the structural performance of rectangular RACFST members with depth-to-width ratios greater than 1.0, especially the slender composite members. To the best of authors' knowledge, only Tam et al. [7] and Yang et al. [25] performed the experimental and finite element analysis (FEA) of the rectangular RACFST stub columns under concentric compression. In addition, based on numerical model taking into account the progressive local buckling and the initial geometric imperfections, Patel et al. [26] and Liang et al. [27] successfully simulated the structural behaviour of uniaxially and biaxially loaded high-strength thin-walled rectangular CFST slender beam-columns. These researches [7, 25-27] provide a good foundation for the study presented in this paper.

The above literature review indicates that there is limited research on the structural performance of rectangular RACFST slender columns under eccentric compression, which is a common loading case in real construction projects. Therefore, the experimental and numerical investigation in this paper are aimed to study the static behaviour of rectangular RACFST slender columns under eccentric compression. The tests of fifteen specimens with different depth-to-width ratio, load eccentricity ratio, slenderness ratio and recycled coarse aggregate (RCA) replacement ratio were performed. Finite element analysis (FEA) model of the eccentrically compressed rectangular RACFST slender columns was built, and further validated by the test results. Moreover, the FEA model was used to reveal the typical failure process and load bearing capacity of rectangular RACFST slender columns under eccentric compression. Simplified equations to predict the bearing capacity of rectangular RACFST slender columns are developed in this paper.

2. Experimental investigation

2.1 Specimens

Fifteen slender column specimens with rectangular cross-section were produced, as summarized in Table 1, where D and B are the outer depth and width of rectangular steel tube, respectively; t is the wall thickness of the steel tube; H is the height of the column; e is the load eccentricity about

major axis of cross-section, $\beta(=D/B)$ is the depth-to-width ratio; $m(=2e/D)$ is the load eccentricity ratio; $\lambda(=2\sqrt{3}H/D)$ is the slenderness ratio about major axis of cross-section; r is the recycled coarse aggregate (RCA) replacement ratio, representing the weight percentage of RCA in the whole coarse aggregate; N_{ue} is the tested bearing capacity; u_{me} is the lateral displacement at the mid-height section when N_{ue} is achieved, and N_{ufea} is the predicted bearing capacity using the FEA model.

The main parameters considered in the experiments include:

- Depth-to-width ratio (β): from 1.0 to 2.0;
- Load eccentricity ratio (m): from 0 to 0.6;
- Slenderness ratio (λ): from 20 to 40; and
- RCA replacement ratio (r): from 0 to 100%.

Rectangular steel tubes were fabricated by welding two identical cold-formed U-shaped profiles using two butt welds, and the sizes and length of the steel tubes were kept in line with the design. Both ends of the rectangular steel tubes were grinded flat, and two rectangular steel endplates with thickness of 16 mm were manufactured in the same time. Before casting the concrete from the upper opening, the lower end of the steel tubes was welded to one endplate, and after completing the concrete casting, the concrete was intentionally left slightly higher than steel tube. After two weeks of concrete curing, the tip of the concrete core was grinded to even to the steel tube with a grinding machine and the top endplate was then welded to the steel tube.

2.2 Material properties

Steel plate with the measured average wall thickness of 2.7 mm was used to produce the rectangular tubes. The properties of steel were obtained on the basis of the customary test on three tensile coupons arbitrarily cut from the steel plates. The measured average yield strength (f_{y}), tensile strength (f_{u}), elastic modulus (E_{s}), yield strain (ε_{y}), Poisson's ratio (μ_{s}) and elongation after fracture (e_{f}) respectively equal to 274.2 MPa, 424.4 MPa, 200.2 GPa, 0.00137, 0.277 and 33.9%, exhibiting the limited discrete.

Three types of concrete mix, including normal concrete (NC) with natural aggregates (i.e. $r = 0$), RAC with r of 50% (RAC1) and RAC with r of 100% (RAC2), were prepared. The RCAs were gained through crushing the waste NC from the same group reinforced concrete members by a jaw crusher, and the cube compressive strength of the original concrete was about 50 MPa. The particle size of RCA ranged from 5 to 25 mm, and the particle gradation, the crushing index, the water absorption ratio, the needle-like particle content, the toughness and the mud content of RCA were all in compliance with the related provisions stipulated in the Chinese standard [28]. The natural coarse aggregates (NCAs) were carbonaceous stone with the same particle size range as the RCAs. The rest of the materials used while producing the concrete included: grade 42.5 Portland cement, natural yellow sand (medium sand), Sika polycarboxylate water reducing agent (WRA) and tap water. These three types of concrete had the same mix proportions for the purpose of comparative studies, as listed in Table 2. The concrete properties, including the cubic compressive strength (f_{cu}), the modulus of elasticity (E_{c}) and the slump height, were respectively obtained by the cube (side lengths of 150 mm) compression test, the prism (side lengths of 150 mm×150 mm×300 mm) compression test and the slump test, and the measured mean values are also included in Table 2, in which $f_{\mathrm{cu,28}}$ and $f_{\mathrm{cu,t}}$ are the average cubic compressive strength at 28-day and during the test day. It can be observed from Table 2 that, the cubic compressive strength, the modulus of elasticity and the slump height of RAC are smaller than those of the reference NC, and RAC with a larger r possesses a worse feature. This is attributed to the fact that, the RCA is rougher than the NCA since the accompanied old mortar with a larger water absorption and a lower strength is attached to the outside of the former [2, 3].

2.3 Tests under eccentric compression

The tests of the specimens under eccentric compression were performed on a 5,000 kN capacity testing machine, and the test set-up and instrumentation are shown in Fig. 1. During the tests, both the upper and lower endplates of the specimen were compressed with the aid of knife hinges acting on the loading plate to replicate the boundary conditions of the hinged ends, and the applied loads were recorded by a load cell placed between the connecting plate of the knife hinge and the top platen

of the testing machine. The equal eccentricity at both ends of the specimen was controlled by the vertical distance between the V-shaped grooves on the loading plate and the cross-sectional centroid. To guarantee sufficient rotation capacity of the endplates, the depth of the V-shaped grooves was made smaller than the height of the knife hinge, and under the same plane the width of the V-shaped grooves was larger than that of the knife hinge. A protecting steel frame was specially fabricated to ensure the safety of the data acquisition equipment during the loading and unloading phases. To track the strain reading on the outer surface of the steel tube at the mid-height section, strain gauges (SGs) were attached in longitudinal and transverse direction at 4 points on the symmetric axis, and SGs were also placed in longitudinal direction at another 4 points close to the tube corner. In addition, 4 displacement transducers (DTs) were set on the bottom platen of the testing machine to record the axial displacements, and another 3 evenly spaced DTs were set along the height of the specimen to capture the lateral displacements.

The tests were carried out using both load-control and displacement-control methods. Before achieving the peak load, the load steps of one tenth to one fifteenth of the estimated bearing capacity were adopted with the loading rate of 0.5 kN/s, and each step was maintained for about 2 minutes. After the peak load reached, the tests were controlled by the axial displacement of the specimen, and the rate of displacement increase was 0.2 mm/min. When the load borne by the specimen dropped to 60% of the peak load, or the lateral displacement at mid-height section was greater than 2% of the specimen height, the tests were ceased.

2.4 Test results and analysis

Similar to those reported in the previous tests [16, 17, 22-24], three stages can be identified for the tested specimens, and good bearing capacity and deformability were observed during the tests. In the first stage, the load and displacement/strain raised approximately linearly and the deformation of the steel tube was not obvious. In the second stage till the peak load, the load and displacement/strain increased nonlinearly with a faster displacement/strain increase, and the compression flange of the steel tube near the mid-height of the column generally began to buckle with the sound of concrete

crushing. In the final stage after the peak load, the load borne by the column decreased rapidly with an increase of the displacement, and the deformation of the buckled steel tube further increased together with the subsequent compressive buckling of the tube side walls.

Fig. 2 demonstrates the failure pattern of the specimens after tests, where the buckled positions of the steel tube are indicated by the arrows. It can be seen that, in general, the local buckling of the steel tube of concentrically compressed columns only occurs along the side walls. This is due to the fact that the tube side walls with a larger width-to-thickness ratio provide a weaker constraint to the concrete core than their neighboring tube flanges. For the eccentrically compressed columns, in general, there is one major local buckling along the compression flange near the mid-height section and several subsequent slight local buckling at the tube side walls along the height, except for the two specimens with a larger slenderness ratio (i.e. B0.3-40-RAC1 and C0.3-36-RAC1), having only one major local buckling of the steel tube at the mid-height section coving compression flange and part of side walls, due to a larger second-order effect under axial compression. However, not all the major local buckling of the steel tube is located near the mid-height of the specimens, which is caused by the material defects variation in a tube. It should be noted that, the local buckling of the steel tube of four eccentrically compressed specimens (i.e. A0.3-30-RAC1, B0.6-30-RAC1, C0.6-30-RAC1 and C0.3-30-RAC2) only happened at one end, which may be induced by the concentration of material defects. Overall, when other parameters keep constant, the peak outward deformation of the major compressive buckling of the steel tube increases with an increase of β, m and λ, and r has a moderate effect, whilst the number of the subsequent local buckling of the tube side walls decreases with a decrease of m and an increase of λ and r, and β has no evident influence.

Typical failure pattern of the concrete core is indicated in Fig. 3. It can be seen that, there is no apparent damage to the concrete core of the concentrically compressed specimens as the steel tube only slightly buckles along the side walls. Moreover, the concrete core of the eccentrically compressed specimens is generally crushed at the major local buckling position of the steel tube, which is similar to the observed phenomena in the previous tests [16, 17, 22, 23], and there is also no

obvious destruction to the concrete core at the subsequent buckling position of the tube side walls. This shows that, in the stage after reaching the peak load, the discrepancy in compressive and flexural deformation induced by the difference in compressive and flexural stiffness between steel tube and concrete core only leads to the subsequent slight local buckling of the tube side walls with a larger D/t ratio, and no new damage to the concrete core happens.

The effect of parameters on the measured load (N) versus axial displacement (δ) relationship of the specimens is shown in Fig. 4, and the axial displacements equal to the mean of the results measured by the four DTs. It can be seen that, the $N-\delta$ curves all include the initial linear and the subsequent nonlinear stage before reaching the peak load and the post-peak descending stage. Generally, the slope of the linear stage of the $N-\delta$ curve decreases with an increase of m, λ and r and increases with an increase of β, due to the increased second-order effect, the decreased E_{c} and the increased area of concrete core. The peak load on the $N-\delta$ curve is defined as the bearing capacity (N_{ue}) of the specimens, which are listed in Table 1.

It was observed from the tests that, except for 2 concentrically compressed specimens and 4 eccentrically compressed specimens possessing local failure at one end, the lateral displacements (u) shape along the height of the eccentrically compressed specimens generally followed half-sine wave curve, as typically demonstrated in Fig. 5, where the solid lines represent the measured results, the dashed lines are the half-sine wave curve with the lateral displacements at the mid-height section equal to the tested values, h is the distance from the bottom end of the specimen, and n (=N/N_{ue}) is the load ratio and negative value of n represents the post-peak phase.

The relationship between load (N) and lateral displacement at the mid-height section (u_{m}) of the specimens changes with the variation of experimental parameters, as demonstrated in Fig. 6. It can be seen that, in general, the initial slope of $N-u_{\mathrm{m}}$ curve decreases, the $N-u_{\mathrm{m}}$ curve enters the nonlinear stage earlier and the load decline rate after the peak reduces with an increase of m, λ and r. This can be attributed to the increased second-order effect with an increase of m and λ, and the decreased E_{c} with increasing r. Moreover, with increasing β, the initial slope of $N-u_{\mathrm{m}}$ curve

increases, the $N-u_{\mathrm{m}}$ curve enters the nonlinear stage earlier and the load decline rate after the peak reduces, due to the increased cross-sectional area of RACFST, the concrete core under tension and the steel tube in tension after the peak load, respectively.

Fig. 7 shows the load (N) versus strain (ε) relationship at the mid-height section of two typical specimens, where the strain at the symmetry points (2 and 4) is averaged, tensile and compressive strains are respectively regarded as positive and negative, and the capital letters 'L' and 'T' in the brackets represent the longitudinal and transverse strain, respectively. It can be seen that, the $N-\varepsilon$ curve has the similar development process as the $N-\delta(u_{\mathrm{m}})$ curve, and it also contains linear and nonlinear phases before the peak load and the post-peak falling phase. Generally, along the side walls of the steel tube, the strain at the corners develops faster than that at the symmetric axis, indicating that the confinement of rectangular steel tube to its concrete core at the corners is stronger than that at the middle of the section, and the compressive strain develops faster than the tensile strain under eccentric compression. Generally, the development of the transverse strains is similar to that of the longitudinal strains, but the signs of them are opposite due to the Poisson effect. For the specimens with a relatively small m, the longitudinal strains at point 3 on the centroid axis are always maintained in compression. Moreover, the specimens with a larger β have a higher strain due to the increased distance from the outermost tube flange to the centroid axis. Based on the detailed analysis of the measured strains, it is found that, the longitudinal strain of the steel tube is approximately linearly distributed along the section depth before reaching the bearing capacity, which means that the mid-height section of the rectangular RACFST slender columns under eccentric compression basically conforms to the 'plane sections remain plane' assumption.

The effect of parameters on load (N) versus longitudinal strain at point 1 ($\varepsilon_{l,1}$) curves is demonstrated in Fig. 8. It can be observed that, $\varepsilon_{l,1}$ of all specimens is far greater than ε_{y} while the peak load achieved, indicating that the ultimate capacity of the tube compression flange can be fully utilized. Furthermore, the impact of each parameter on the development of the rising stage of the $N-\varepsilon_{l,1}$ curve before the peak load is basically the same as that of the $N-\delta(u_{\mathrm{m}})$ curve. However,

the influence of each parameter on the development of the post-peak descending stage of the $N-\varepsilon_{l,1}$ curve is more ambiguous. This is mainly due to the fact that, the major local buckling portion of the steel tube of several specimens does not occur at point 1, resulting in constant or even reduce of strain with a decrease of loads.

Fig. 9 shows the influence of parameters on the measured bearing capacity (N_{ue}). It can be seen that, N_{ue} of the specimens with the same B value increases with increasing β due to the increased cross-sectional area, and N_{ue} of the specimens with β of 1.5 and 2.0 is 1.3 times and 1.67 times of that with β of 1.0 (square one). While keeping other parameters constant, N_{ue} of the specimens decreases with an increase of m, λ and r due to the increased second-order effect and the decreased concrete strength. Overall, m has most obvious influence on N_{ue}, followed by λ, indicating that the load eccentricity and the second-order effect are the main factors determining the bearing capacity of a rectangular RACFST slender column. The specimens with m of 0.3 and 0.6 respectively result in 26.6~50.6% ($\beta=1.5$) and 11.2~36.4% ($\beta=2.0$) lower N_{ue} than those with m of zero, and N_{ue} of the specimens with λ of 30 and 40/36 is 4.1~12.5% ($\beta=1.5$) and 7.9~8.4% ($\beta=2.0$) lower than that of the specimens with λ of 20, respectively. However, r has a relatively small effect on N_{ue} as the confinement of the steel tube alleviates the degree of the decrease of the core RAC strength with increasing r, which is similar to the findings in previous studies [7, 19]. When r is increased from zero to 50% and 100%, 1.0~2.8% ($\beta=1.5$) and 3.9~10.9% ($\beta=2.0$) lower N_{ue} is respectively produced.

The effect of parameters on the lateral displacement at the mid-height while achieving N_{ue} (u_{me}) is demonstrated in Fig. 10. It is shown that, while keeping the remaining parameters constant, u_{me} generally increases with an increase of β, m and λ mainly due again to the increased second-order effect. The specimens with β of 1.5 and 2.0 respectively possess 56% and 98% larger u_{me} than the corresponding specimen with β of 1.0, and u_{me} of the specimens with λ of 30 and 40/36 are 2.7~3.7 times ($\beta=1.5$) and 2.5~3.1 times ($\beta=2.0$) of that of the specimens with $\lambda=20$, respectively. However, the concentrically compressed specimens have a very small u_{me}, which is

about 13% ($\beta = 1.5$) and 8% ($\beta = 2.0$) of that of the corresponding eccentrically compressed specimens. Moreover, take $r = 50\%$ as the boundary, u_{me} increases first and then decreases with increasing r. The increased u_{me} is attributed to the decreased E_{c} when $r \leq 50\%$; however, more defects in the RAC may cause premature destruction of the specimens when $r = 100\%$. Generally, when r is increased from zero to 50% and 100%, about 4.5% larger and 2.0% lower u_{me} is produced.

The impact of parameters on $\varepsilon_{\mathrm{ue},l}/\varepsilon_{\mathrm{y}}$ is shown in Fig. 11, where $\varepsilon_{\mathrm{ue},l}$ is the longitudinal strain recorded at each measuring point while reaching N_{ue}. It is shown that, for the concentrically compressed specimens, the compressive strains of the measuring points are almost approximative regardless of β value. This is generally consistent with the failure characteristics of the specimens, i.e. there is no obvious lateral displacement occurred at the mid-height section (see Fig. 2(b)). For the eccentrically compressed specimens, the mid-height section of the column has both compressive and tensile portion, and the cross-sectional centroid axis (point 3) is in the compressive portion while reaching N_{ue}. The strain of the compression flange of the steel tube is fully developed, and $\varepsilon_{\mathrm{ue},l}$ at the corner (point 2) is larger than that at the symmetry axis (point 1). The calculated results show that $\varepsilon_{\mathrm{ue},l}$ of the compression flange of the steel tube is about 2~6 times of ε_{y}. The longitudinal strain of the tension flange of the steel tube is not fully developed as the cross-section at the mid-height is mainly under compression, and the strain difference between the corner (point 4) and the symmetry axis (point 5) is not obvious. At the same time, there are only a few cases in which $\varepsilon_{\mathrm{ue},l}$ of the tube tension flange is greater than ε_{y}.

3. Numerical simulation

3.1. Finite element analysis (FEA) model

In order to simulate the behaviour of the eccentrically compressed rectangular RACFST slender columns, a three-dimensional nonlinear finite element analysis (FEA) model was established using ABAQUS software [29].

The adopted constitutive model for the steel tube and the concrete core consisted of both elastic

and plastic stages of the material. The elastic modulus and the Poisson's ratio of steel were obtained from tensile coupon tests, and those of concrete were set to be $4730\sqrt{f_c'}$ [30] and 0.2 [25] respectively, where f_c' is the cylinder compressive strength of concrete converted from $f_{\mathrm{cu,t}}$ according to the provisions in [31]. In simulating the plasticity of steel a classical metal plasticity model in ABAQUS [29] was used, with the true stress versus plastic strain relationship derived from the nominal one for the cold-formed steel suggested in [32], and the inelastic behaviour of concrete core was modelled by the damaged plasticity model in ABAQUS [29], with the yield and failure surface controlled by the equivalent plastic strain and the stiffness degradation characterized by the damage variables. To obtain the compressive stress-inelastic strain data of the RAC core in rectangular steel tube, the nominal compressive stress-strain relationship in [25] was adopted, and thus the influence of the confinement of rectangular steel tube to the RAC core on the post-peak phase of the compressive stress-strain relationship was considered. Moreover, the fracture energy cracking criterion was utilized to specify the tension stiffening of the core RAC.

Four-node reduced integration shell elements (S4R) were employed to model the rectangular steel tube, and eight-node reduced integration linear brick elements (C3D8R) were adopted to simulate the concrete core and two endplates. The final mesh density was determined based on the difference of the simulated bearing capacity between two adjacent meshes within 1%. For the main contact between the inner surface of the tube and the concrete core, the hard contact and the Coulomb friction with a friction coefficient of 0.6 [25] were defined in the normal direction and the tangential directions, respectively. In addition, the contact (welding) between the tube ends and the endplates was defined as the shell-brick coupling constraints, and the normal contact between the concrete core and the end plate was set as hard contact while ignoring the tangential contact.

The FEA model of rectangular RACFST slender columns under eccentric compression is demonstrated in Fig. 12. To replicate the function of the knife hinge (see Fig. 1), a loading line was set on each of the upper and lower endplates, and the perpendicular distance from the loading line to the cross-sectional centroid axis was equal to the load eccentricity (e) in the tests. Moreover, a load

eccentricity of $H/1000$ was employed to consider the effect of the initial geometric imperfection of the columns [21, 26, 27]. Boundary conditions of the FEA model are shown in Fig. 12. In the initial analysis step, all displacements of the loading line on the lower endplate were restricted, and the translations in X and Y directions of the loading line on the upper endplate were restricted. In the follow-up analysis step, an axial displacement (δ) of 50 mm along the Z direction was exerted to the loading line on the upper endplate of the column.

3.2. Verification of the FEA model

The predicted typical failure pattern of typical specimens together with the Mises stress of the steel tube are shown in Fig. 13. It can be found from the comparison between Fig. 13 and Fig. 2 that, except for the four aforementioned eccentrically compressed specimens with one end buckling of the steel tube, the predicted results generally represent the behaviour of the specimens, i.e. the local buckling of the steel tube of the concentrically compressed columns mainly occurs near the ends, while the local buckling of the steel tube (including compression flange and part of side walls) of the eccentrically compressed columns is mainly concentrated near the mid-height section. However, there is a certain difference between the simulated and observed buckling position of the tube, because the steel tube and its concrete core in the FEA model are simulated using idealized materials model, while the materials of the test specimens have randomly distributed defects. Moreover, the Mises stresses of the steel tube of the eccentrically compressed columns is generally attenuated from the mid-height section to both ends, indicating that the final failure of the rectangular RACFST slender columns under eccentric compression is controlled by the destruction of the mid-height section. Fig. 14 demonstrates the predicted typical failure pattern together with the logarithmic strain along the vertical direction (LE33) of the concrete core in the steel tube. According to the contrast between Fig. 14 and Fig. 3, it can be discovered that, the concrete destruction of the eccentrically compressed column is generally concentrated on 1~2 positions near the mid-height section, and the compressive LE33 at the major local buckling position of the tube compression flange is the largest. In addition, the concrete core of the concentrically compressed column also shows local failure near the ends.

The comparison between the predicted and measured $N-u_{\mathrm{m}}$ curves is depicted in Fig. 6. It can be seen that, both curves have the similar trend although the simulated initial slope, the bearing capacity and the descending stage after the peak are slightly different from the measured results; however, the four aforementioned eccentrically compressed specimens with one end failure show a larger difference. The divergence between the predicted and measured $N-u_{\mathrm{m}}$ curves may because of the existence of initial defects, such as the difference between the properties of the materials in the composite specimens and those measured by the concrete blocks and steel coupons, initial cracks in the concrete core, possible gap between steel tube and core concrete, and the difference between the simulated and observed steel tube buckling position and/or range after the peak load. Fig. 8 shows the typical comparison between the simulated and recorded $N-\varepsilon_{l,1}$ curves of the specimens. It can be seen that, before reaching the peak load, the predicted $N-\varepsilon_{l,1}$ curves generally agree well with the recorded ones. However, after achieving the peak load, the simulated curves are unloaded at a constant slope as the strain increases, showing a significant difference from the measured ones. This can be explained by that, point 1 in the FEA model is exactly the buckling position of the tube compression flange, whilst point 1 on the specimens is generally not the exact position where the steel tube is buckled under compression. The predicted bearing capacities (N_{ufea}) by the FEA model are compared with N_{ue} in Fig. 15 and Table 1. Analysis on the data indicates that, the mean and standard deviation of $N_{\mathrm{ufea}}/N_{\mathrm{ue}}$ are equal to 0.989 and 0.044, respectively, and the discrepancy between N_{ufea} and N_{ue} is within 10%. This demonstrates that the predicted bearing capacities of rectangular RACFST slender columns under eccentric compression using the FEA model generally accord well with the measured results.

Although there are divergences between the predicted load (N) versus deformation (u_{m} and $\varepsilon_{l,1}$) curves and the measured results, the predicted failure patterns, bearing capacities as well as development trend of lateral displacements and strains at the mid-height section are generally in good agrement with the recorded results. Therefore, it can be considered that the FEA model built in this study is capable of well simulating the performance of rectangular RACFST slender columns under

eccentric compression.

3.3. Mechanism analysis using the FEA model

Based on the validated FEA model, the investigation into the typical mechanism of rectangular RACFST slender columns under eccentric compression was carried out. The geometric and physical conditions of the benchmark composite member included: $D \times B = 480 \times 320$ mm ($\beta = 1.5$), $m = 0.5$, $\lambda = 40$, $r = 50\%$, steel ratio $\alpha = 0.1$, $f_y = 355$ MPa, and $f_c' = 50$ MPa, where α is the ratio of cross-sectional area of steel to that of concrete core. In addition, to ensure comparability, the cross-sectional area of the composite member was kept constant when β was varied.

The simulated results indicated that, except for the composite columns with a relatively small m and λ, the concrete core at the mid-height section of the column had both tension and compression zone, and when other parameters kept constant the sectional height of the tension zone increased with an increase of β, m, λ, f_y and f_c' and a decrease of α, whilst r had a moderate impact. The highest longitudinal stress of the core RAC higher than f_c' appeared at the corner of the compression zone due to a stronger constraint from the steel tube. Furthermore, the maximum longitudinal stress of the core RAC at the corner lessened with a growing of β, λ and r and a lowering of m, α, f_y and f_c'. The influence of typical parameters on longitudinal stress of core RAC (S33) at the mid-height section of the column while achieving the bearing capacity is shown in Fig. 16.

Typical variation of interaction stress between the steel tube and the concrete core (p) at the mid-height section of the column with the increase of u_m is demonstrated in Fig. 17, where the triangles represent the moment when the column reaches its bearing capacity. It can be seen that, under the same u_m, p at the corners of the section (points b and d) are significantly higher than those at other points, and before reaching the bearing capacity the difference of p between points b and d is not apparent. However, after the bearing capacity is achieved p of point d gradually exceeds that of point b owing to the local buckling of steel tube near point b. The interaction stress (p) at the mid-point of the tube tension flange (point f) is quite small, and p at points a and c are close to zero due mainly to the separation between the steel tube and the concrete core caused by the local buckling of

the steel tube. These indicate that the interaction between the steel tube and the concrete core is mainly distributed at the corners of the section. The effect of key parameters on $p-u_{\mathrm{m}}$ relationship at point b is presented in Fig. 18. It is shown that, under the same u_{m}, p decreases with an increase of β, m and λ due to the increased second-order effect. However, r has a moderate effect on the development of $p-u_{\mathrm{m}}$ relationship.

4. Simplified formulae

To obtain the simplified formulae for the bearing capacity prediction of rectangular RACFST slender columns under eccentric compression, parametric analysis on the axial load ratio (N/N_0) versus the moment ratio (M/M_{u}) relationship was performed using the FEA model, where N and M are the applied axial compressive load and moment respectively, and M equals to $N\cdot e$; N_0 and M_{u} are the cross-sectional strength and moment capacity, respectively. The simulation results indicated that, for the N/N_0 versus M/M_{u} relationship, the influence of α, f_{y} and f_{c}' could be unified as the effect of the confinement factor (ξ_{r}) [12]. The impact of β, r, ξ_{r} and λ on the N/N_0 versus M/M_{u} relationship is plotted in Fig. 19 by the solid lines. It can be seen that, while keeping other parameters constant, the bearing capacity of the column decrease with an increase of r and λ and a decrease of ξ_{r}, and β generally has a moderate effect on the bearing capacity of the column.

A large number of numerical simulations and further date analysis showed that the simplified N/N_0 versus M/M_{u} correlation equations for square RACFST slender columns under eccentric compression in [12] were also suitable for rectangular ones, and the formulae are as follows:

$$\begin{cases} \dfrac{N}{\varphi N_0}+\dfrac{a}{d}\dfrac{M}{M_{\mathrm{u}}}=1 & \left(\dfrac{N}{N_0}\geq 2\varphi^3\eta_0\right) \\ -b\left(\dfrac{N}{N_0}\right)^2-c\dfrac{N}{N_0}+\dfrac{1}{d}\dfrac{M}{M_{\mathrm{u}}}=1 & \left(\dfrac{N}{N_0}<2\varphi^3\eta_0\right) \end{cases} \tag{1}$$

where, φ is the stability factor, a, b, c and η_0 are the intermediate variables, and d is the factor considering the second-order effect. The specific simplified formulae for N_0 and M_{u} are detailed in [12].

The simplified N/N_0 versus M/M_{u} relationship indicated by the dashed lines are also presented

in Fig. 19. It can be seen that both the simplified and FEA curves have the same trend and similar predictions. Fig. 20 demonstrates the effect of β and r on $N_{\mathrm{us}}/N_{\mathrm{ue}}$ of rectangular RACFST slender columns under eccentric compression, where N_{us} is the simplified bearing capacity, and the effective test data in this study and those from the literatures (58 in total) are covered in the comparison. It can be found that a suitable fitness between the simplified and experimental bearing capacities is attained, considering that the mean and standard deviation of $N_{\mathrm{us}}/N_{\mathrm{ue}}$ equal to 0.907 and 0.111, respectively. The application scope of the simplified equations is: $\beta = 1.0\sim2.0$, $r = 0\sim100\%$, $\alpha = 0.05\sim0.2$, $f_{\mathrm{y}} = 200\sim500$ MPa, and $f_{\mathrm{c}}' = 25\sim65$ MPa.

5. Conclusions

Based on the experimental and numerical studies on the eccentrically compressed rectangular RACFST slender columns, the following conclusions can be drawn:

(1) After completing the tests, the eccentrically compressed rectangular RACFST slender columns generally have local buckling observed in compression flange and part of side walls of the steel tube near the mid-height section, and the columns with a larger β, m and λ possess a larger peak outward deformation of the steel tube at the major local buckling portion. Generally, the concrete core is crushed at the major local buckling portion of the steel tube.

(2) The load (N) versus deformation (δ, u_{m} and ε) curve of rectangular RACFST slender column specimens under eccentric compression consists of initial linear and the subsequent nonlinear stages before reaching the peak load and the post-peak descending stage. Generally, the initial slope of the load versus deformation curve decreases with an increase of m, λ and r and a decrease of β.

(3) When other parameters keep constant, the columns with a larger m, λ and r tend to have a lower N_{ue}, while those having a larger β end up with a higher N_{ue}. Overall, compared with the smallest β, m, λ and r values (1.0, 0, 20 and 0), the columns with a larger β, m, λ and r result in 30~67% higher, 11.2~50.6% lower, 4.1~12.5% lower and 1.0~10.9% lower N_{ue}, respectively.

(4) The simulated responses of rectangular RACFST slender columns under eccentric compression using the established FEA model generally agree well with the experimental observations. Parametric

analysis results reveal the impact of key factors on the mechanism of the eccentrically compressed rectangular RACFST slender columns.

(5) The simplified equations for the axial load ratio versus moment ratio of rectangular RACFST slender columns under eccentric compression are suggested, from which the calculated bearing capacities are in good agreement with the experimental results.

Declaration of Competing Interest

The authors declare that they have no known competing financial interests or personal relationships that could have appeared to influence the work reported in this paper.

Acknowledgements

The studies in this paper are financially supported by the National Natural Science Foundation of China (Grant No. 51678105). The financial support is gratefully acknowledged.

References:

[1] J. Nobre, M. Bravo, J. de Brito, G. Duarte, Durability performance of dry-mix shotcrete produced with coarse recycled concrete aggregates, Journal of Building Engineering 29 (2020) 101135.

[2] T. C. Hansen, Recycling of Demolished Concrete and Masonry, Report of RILEM TC 37-DRC on Demolition and Reuse of Concrete, E&FN Spon, London, UK, 1992.

[3] E. Vázquez, Progress of Recycling in the Built Environment, Final Report of the RILEM Technical Committee 217-PRE, Springer, Heidelberg, Germany, 2013.

[4] V. W. Y. Tam, M. Soomro, A. C. J. Evangelista, A review of recycled aggregate in concrete applications (2000-2017), Construction and Building Materials 172 (2018) 272-292.

[5] K. Konno, Y. Sato, Y. Kakuta, M. Ohira, Property of recycled concrete column encased by steel tube subjected to axial compression, Transactions of the Japan Concrete Institute 19(2) (1997) 231-238.

[6] Y. F. Yang, L. H. Han, Compressive and flexural behaviour of recycled aggregate concrete filled steel tubes (RACFST) under short-term loadings, Steel and Composite Structures 6(3) (2006) 257-284.

[7] V. W. Y. Tam, Z. B. Wang, Z. Tao, Behaviour of recycled aggregate concrete filled stainless steel stub columns, Materials and Structures 47(1-2) (2014) 293-310.

[8] W. Li, J. Xiao, C. Shi, C. S. Poon. Structural behaviour of composite members with recycled aggregate concrete-an overview, Advances in Structural Engineering 18(6) (2015) 919-938.

[9] L. H. Han, W. Li, R. Bjorhovde, Developments and advanced applications of concrete-filled steel tubular (CFST) structures: Members, Journal of Constructional Steel Research 100 (2014) 211-228.

[10] Y. Du, Z. Chen, J. Y. R. Liew, M. X. Xiong, Rectangular concrete-filled steel tubular beam-columns using high-strength steel: Experiments and design, Journal of Constructional Steel Research 131 (2017) 1-18.

[11] X. L. Zhao, L. H. Han, H. Lu, Concrete-Filled Tubular Members and Connections, Taylor and Francis, Oxford, UK, 2010.

[12] Y. F. Yang, C. Hou, Behaviour and design calculations of recycled aggregate concrete filled steel tube (RACFST) members, Magazine of Concrete Research 67(11) (2015) 611-620.

[13] J. Chen, Y. Wang, C. W. Roeder, J. Ma, Behavior of normal-strength recycled aggregate concrete filled steel tubes under combined loading, Engineering Structures 130 (2017) 23-40.

[14] W. Q. Lyu, L. H. Han, Investigation on bond strength between recycled aggregate concrete (RAC) and steel tube in RAC-filled steel tubes, Journal of Constructional Steel Research 155 (2019) 438-459.

[15] V. W. Y. Tam, J. Xiao, S. Liu, Z. Chen, Behaviors of recycled aggregate concrete-filled steel tubular columns under eccentric loadings, Frontiers of Structural and Civil Engineering 13(3) (2019) 628-639.

[16] Y. F. Yang, L. H. Han. Experimental behaviour of recycled aggregate concrete filled steel tubular columns, Journal of Constructional Steel Research 62(12) (2006) 1310-1324.

[17] Z. Chen, S. Zheng, Q. Li, J. Xue, B. Chen, Experimental study on behavior of recycled aggregate concrete filled square steel tubular long columns under eccentric compression loading, Journal of Building Structures 33(9) (2012) 21-29. (in Chinese)

[18] Z. Chen, C. Jing, J. Xu, X. Zhang, Seismic performance of recycled concrete-filled square steel tube columns, Earthquake Engineering and Engineering Vibration 16(1) (2017) 119-130.

[19] Y. F. Yang, G. L. Ma. Experimental behaviour of recycled aggregate concrete filled stainless steel tube stub columns and beams, Thin-Walled Structures 66 (2013) 62-75.

[20] Y. F. Yang, Z. C. Zhang, F. Fu, Experimental and numerical study on square RACFST members under lateral impact loading, Journal of Constructional Steel Research 111 (2015) 43-56.

[21] Y. F. Yang, L. Zhang, X. Dai, Performance of recycled aggregate concrete filled square steel tubular columns exposed to fire, Advances in Structural Engineering 20(9) (2017) 1340-1356.

[22] N. Hu, X. Du, P. Liu, Z. Niu, Experimental study on mechanical behavior of recycled aggregate concrete-filled square steel tubular long columns under eccentric compression loading, Journal of Building Structures 37(Suppl. 2) (2016) 36-42. (in Chinese)

[23] Y. Xu, Y. Yao, Z. Zhang, D. Chen, Experimental research on mechanical behavior of recycled aggregate concrete filled square steel tubular long columns under eccentric compression loading,

Building Structure 46(9) (2016) 69-74. (in Chinese)

[24] X. Yu, C. Wang, B. Liu, Q. Hu, J. Chen, Experimental study of the behavior of recycled aggregate concrete filled square steel tubular long columns under eccentric compression, Journal of Hefei University of Technology 40(8) (2017) 1110-1116. (in Chinese)

[25] Y. F. Yang, C. Hou, M. Liu, Tests and numerical simulation of rectangular RACFST stub columns under concentric compression, Structures 27 (2020) 396-410.

[26] V. I. Patel, Q. Q. Liang, M. N. S. Hadi, High strength thin-walled rectangular concrete-filled steel tubular slender beam-columns, Part I: Modeling, Journal of Constructional Steel Research 70 (2012) 377-384.

[27] Q. Q. Liang, V. I. Patel, M. N. S. Hadi, Biaxially loaded high-strength concrete-filled steel tubular slender beam-columns, Part I: Multiscale simulation, Journal of Constructional Steel Research 75 (2012) 64-71.

[28] GB/T 25177, Recycled Coarse Aggregate for Concrete, Standards Press of China, Beijing, 2010. (in Chinese)

[29] Simulia, ABAQUS 6.14 Analysis User's Manual, Dassault Systemes Simulia Corp., Providence, RI, USA, 2014.

[30] ACI Committee 318, ACI 318-19 — Building Code Requirements for Structural Concrete and Commentary, American Concrete Institute, Farmington Hills, Michigan, USA, 2019.

[31] CEN, EN 1992-1-1. Eurocode 2: Design of Concrete Structures—Part 1-1: General Rules and Rules for Buildings, 2004.

[32] N. Abdel-Rahman, K. S. Sivakumaran, Material properties models for analysis of cold-formed steel members, Journal of Structural Engineering ASCE 123(9) (1997) 1135-1143.

Figures:

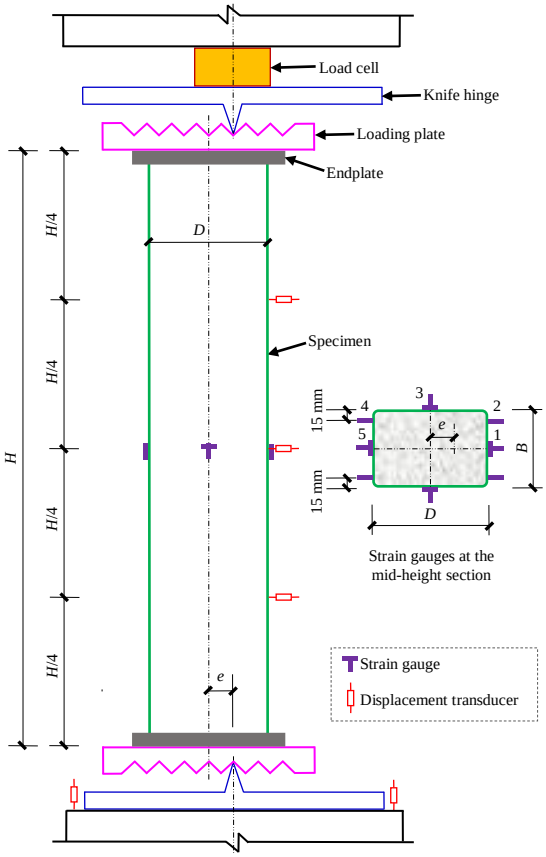

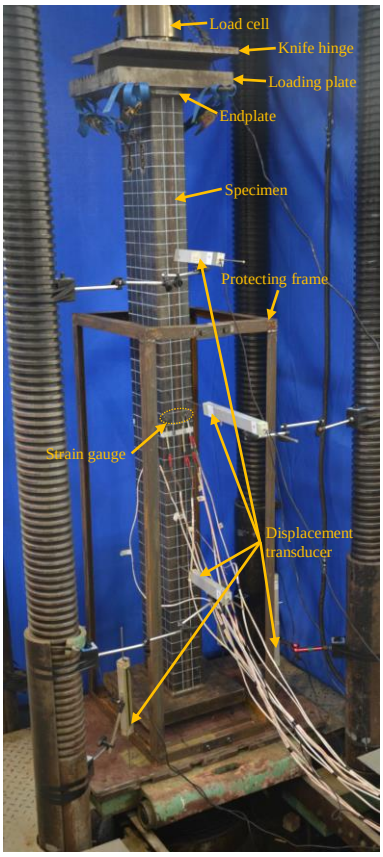

(a) Schematic view (b) Real scenario

Fig. 1. Test set-up and instrumentation.

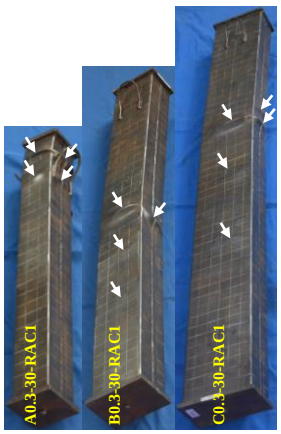

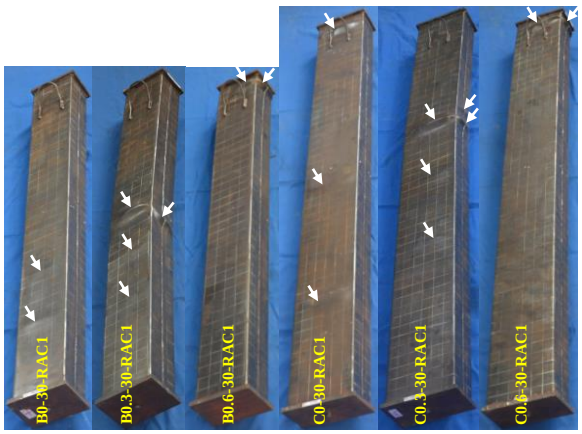

(a) Variation of β (b) Variation of m

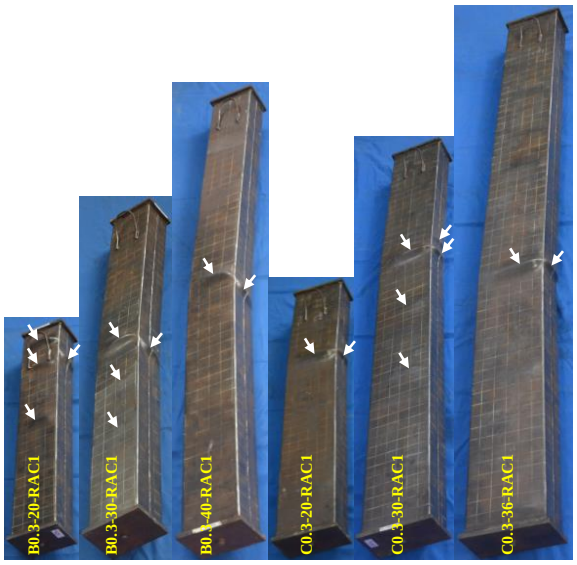

(c) Variation of λ

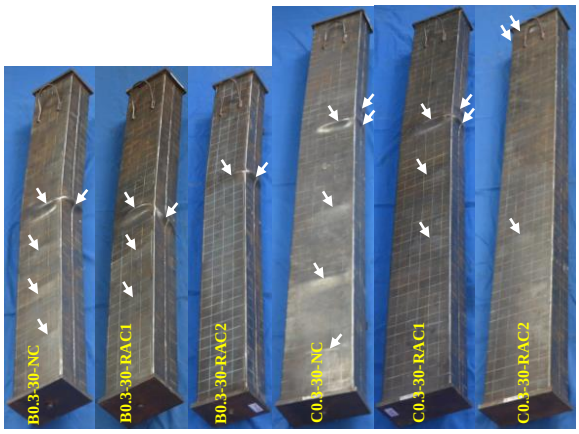

(d) Variation of r

Fig. 2. Failure pattern of the specimens.

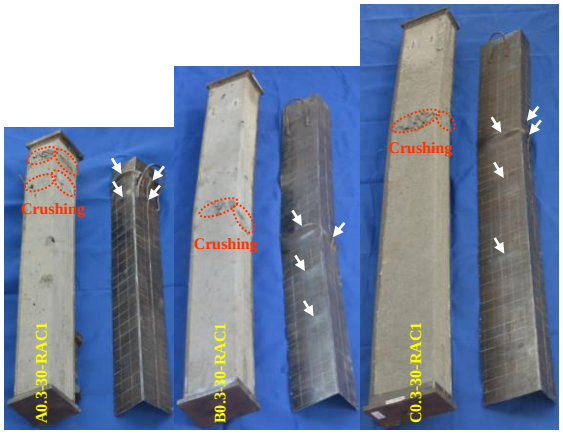

(a) Variation of β

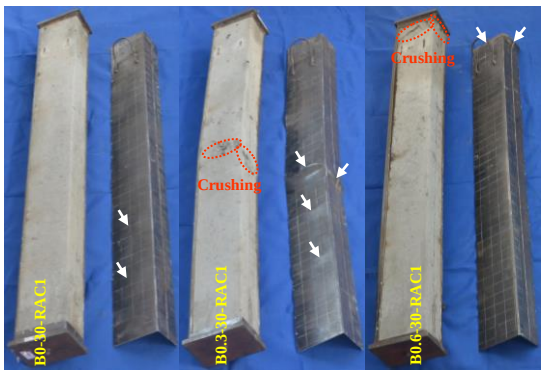

(b) Variation of m

(c) Variation of λ

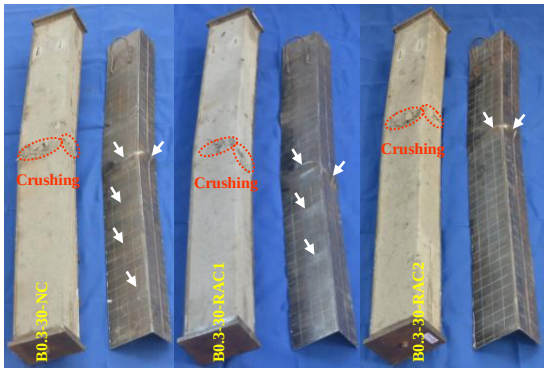

(d) Variation of r

Fig. 3. Typical failure pattern of the concrete core.

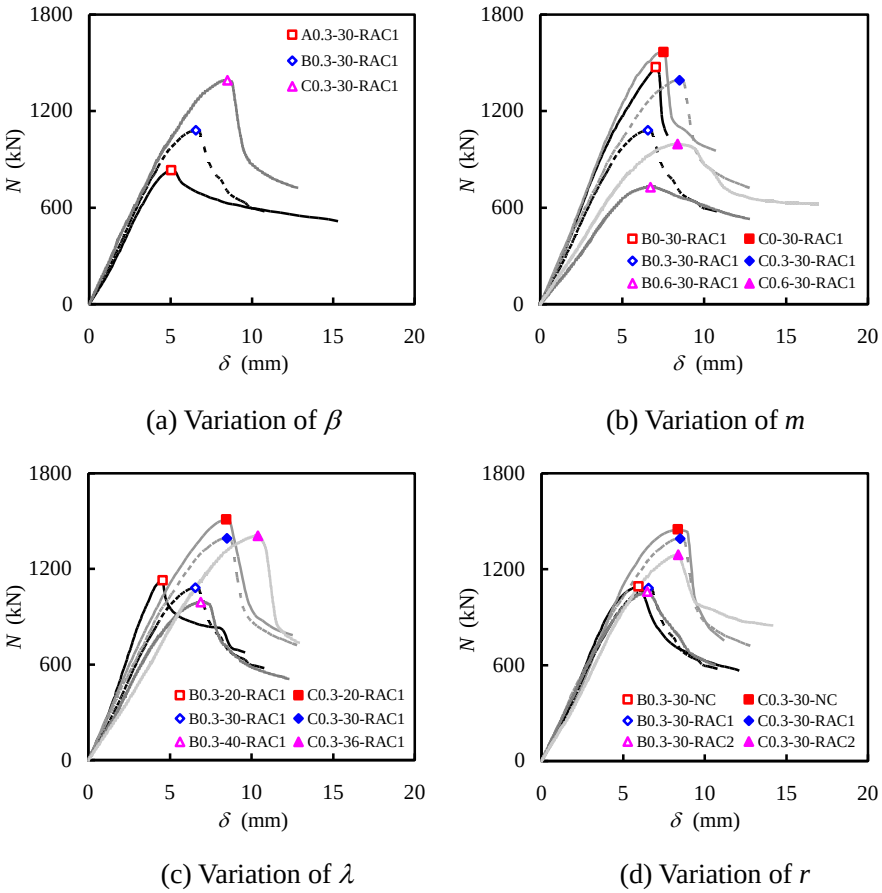

(a) Variation of β (b) Variation of m

(c) Variation of λ (d) Variation of r

Fig. 4. Load (N) versus axial displacement (δ) relationship of the specimens.

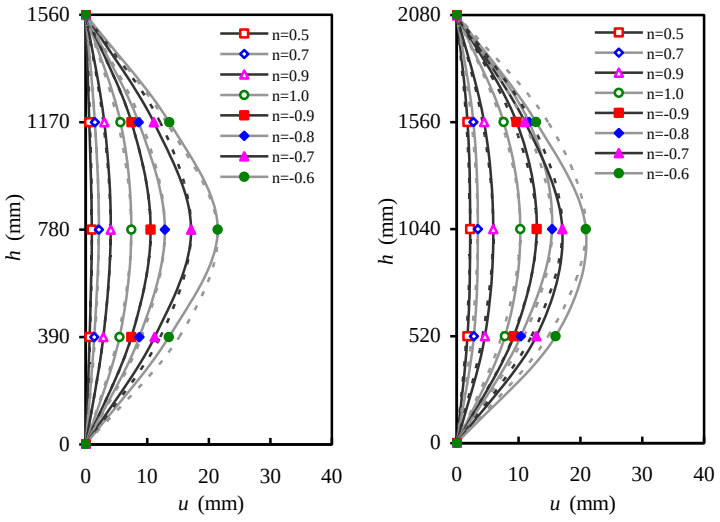

(a) B0.3-30-RAC1 (b) C0.3-30-RAC1

Fig. 5. Representative lateral displacements of the specimens.

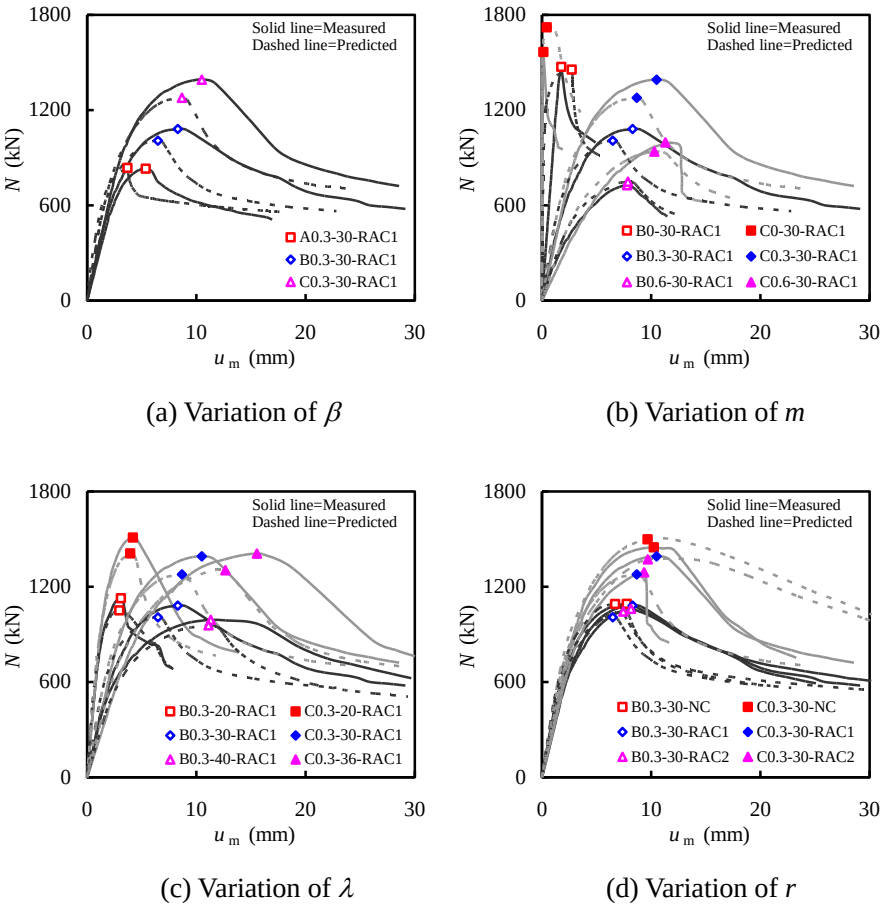

(a) Variation of β (b) Variation of m

(c) Variation of λ (d) Variation of r

Fig. 6. Load (N) versus lateral displacement at the mid-height section (u_m) curves.

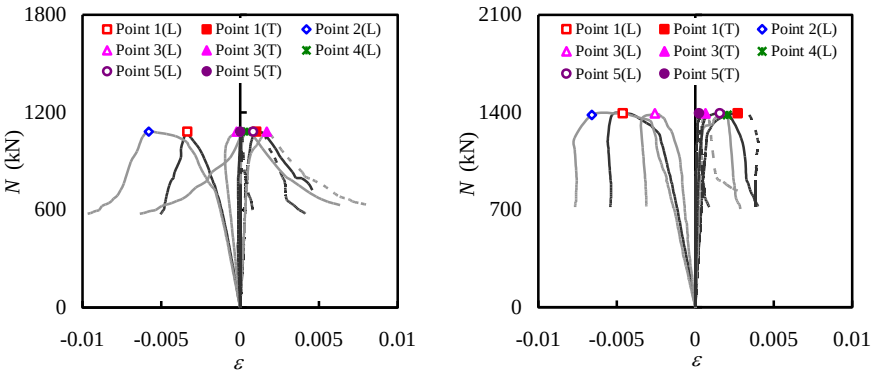

(a) B0.3-30-b (b) C0.3-30-b

Fig. 7. Load (N) versus strain (ε) relationship of typical specimens.

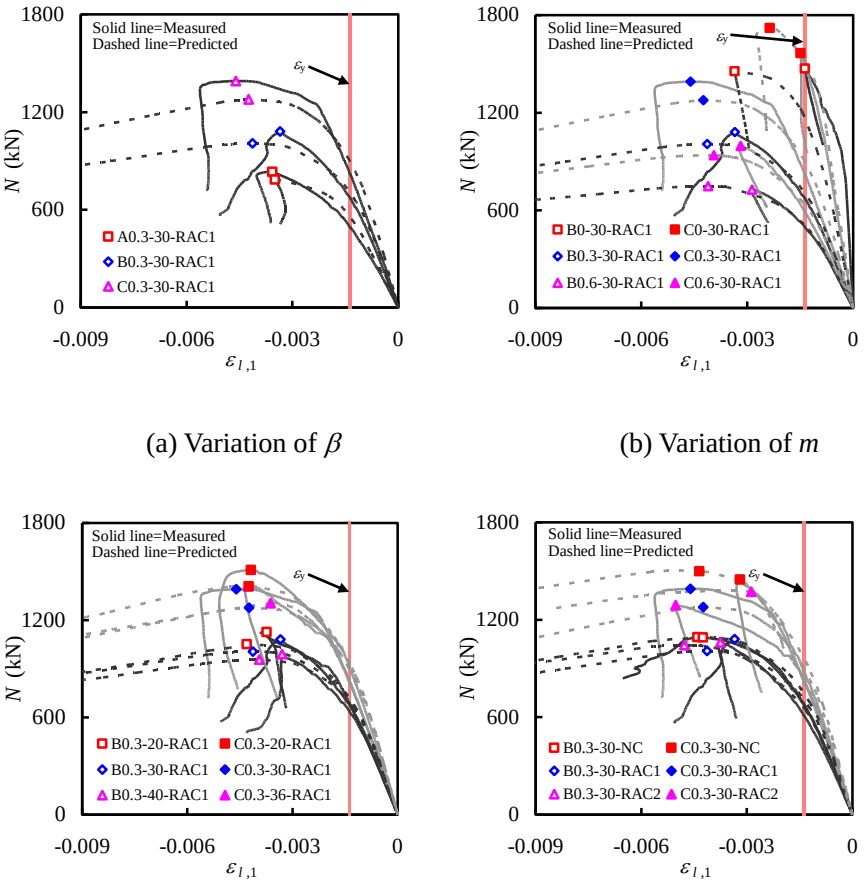

(a) Variation of β

(b) Variation of m

(c) Variation of λ

(d) Variation of r

Fig. 8. Effect of parameters on load (N) versus longitudinal strain at point 1 ($\varepsilon_{l,1}$) curves.

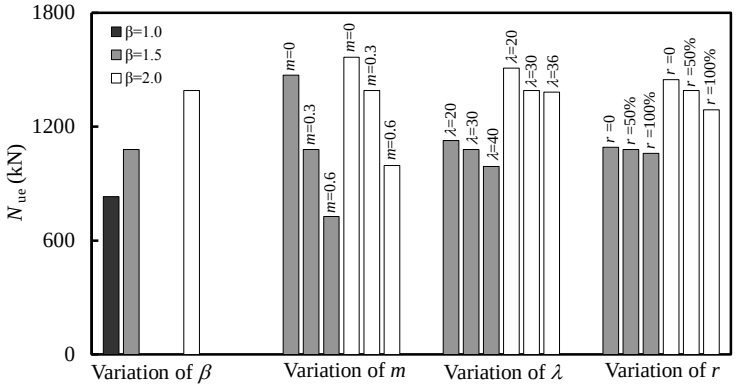

Fig. 9. Influence of parameters on N_{ue}.

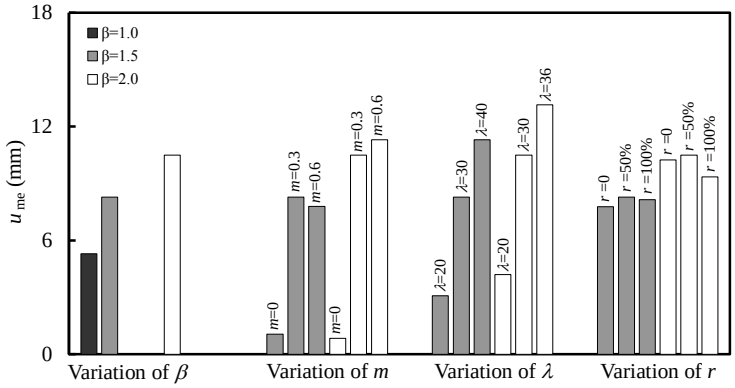

Fig. 10. Effect of parameters on u_{me}.

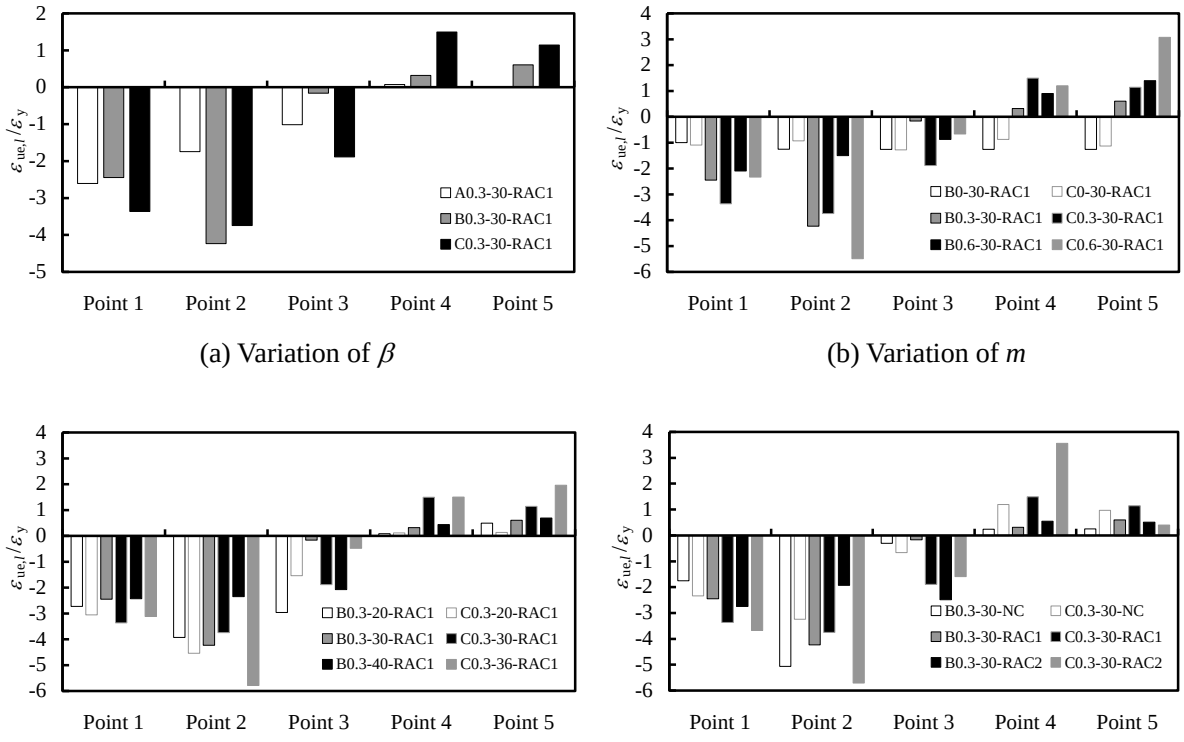

(a) Variation of β

(b) Variation of m

(c) Variation of λ

(d) Variation of r

Fig. 11. Impact of parameters on $\varepsilon_{ue,l}/\varepsilon_y$.

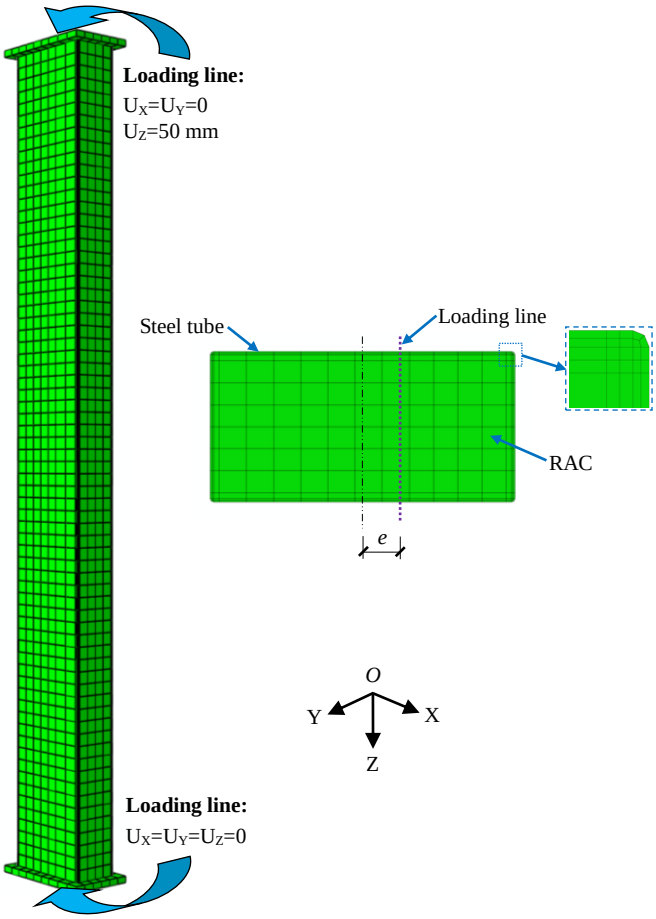

Fig. 12. FEA model of rectangular RACFST slender columns under eccentric compression.

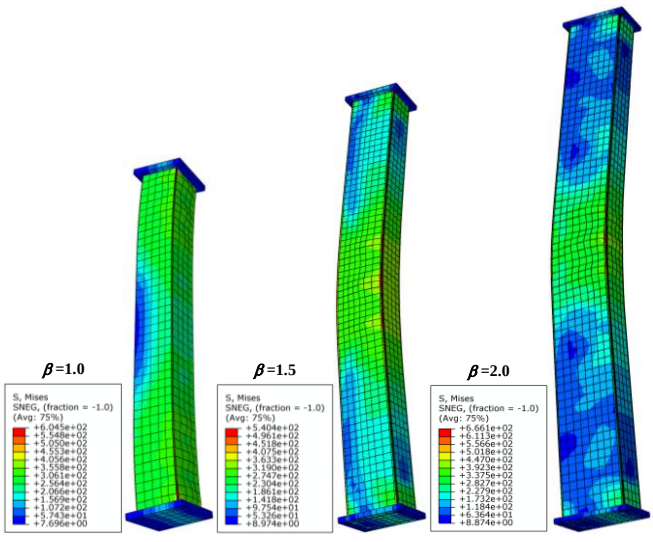

(a) Variation of β

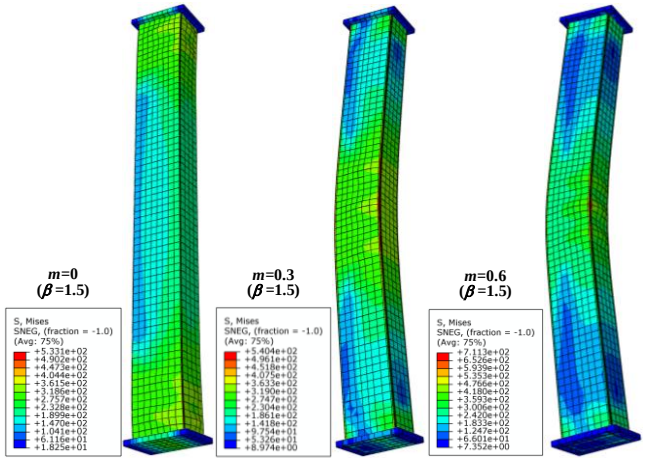

(b) Variation of m

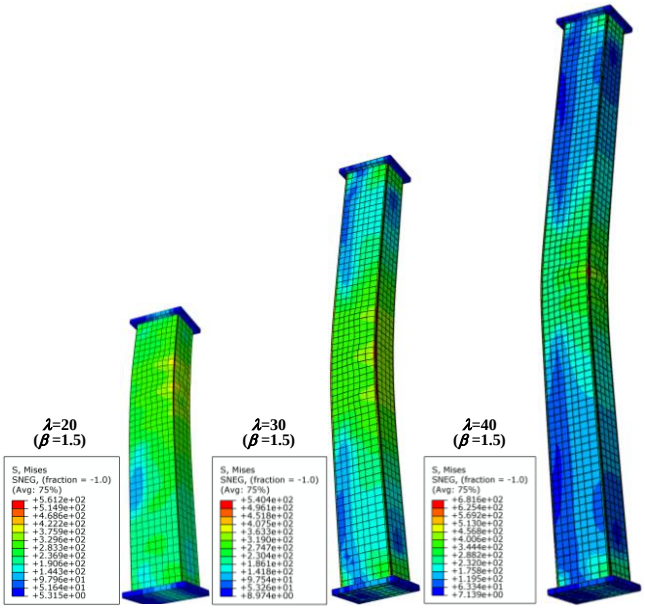

(c) Variation of λ

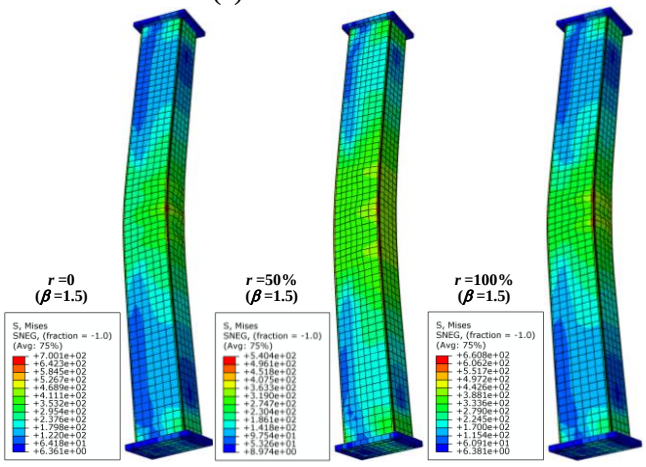

(d) Variation of r

Fig. 13. Predicted failure pattern of typical specimens.

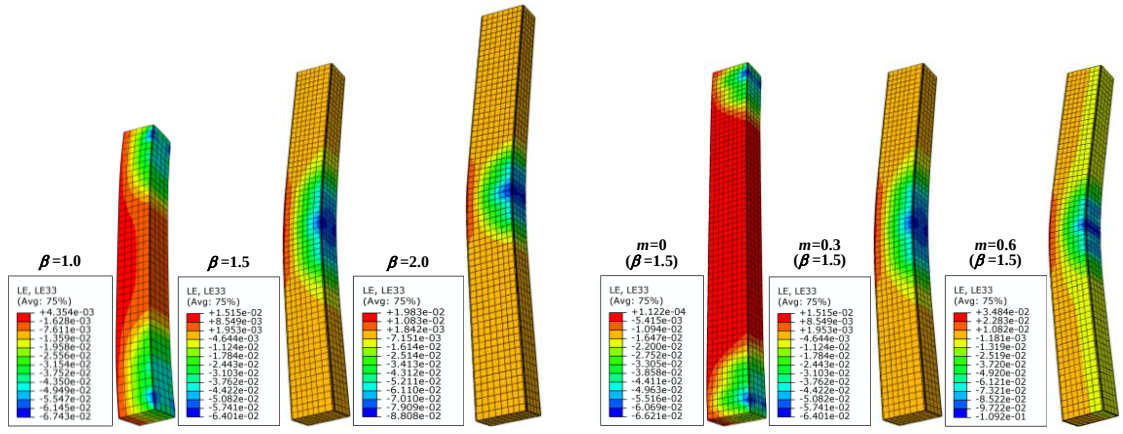

(a) Variation of β (b) Variation of m

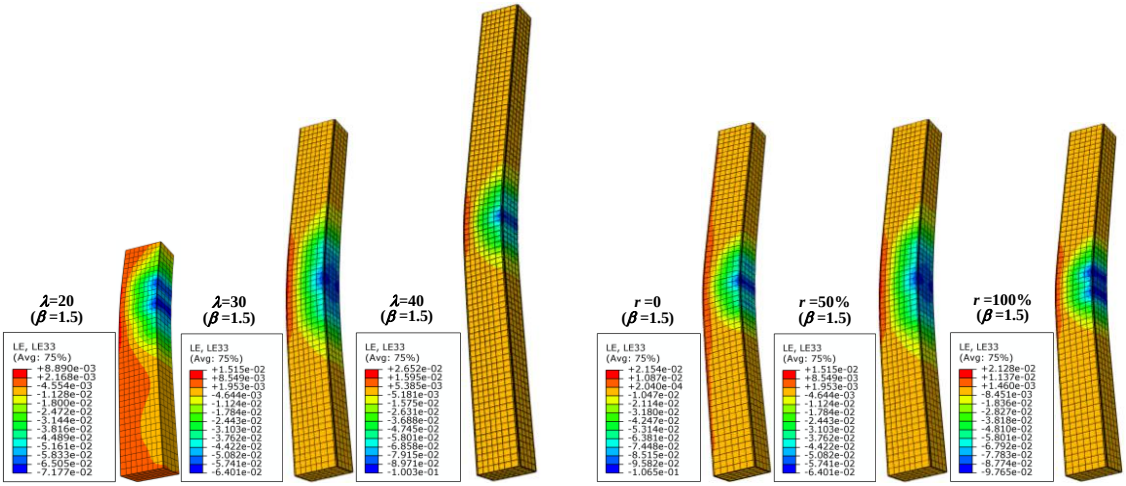

(c) Variation of λ (d) Variation of r

Fig. 14. Predicted typical failure pattern of the concrete core.

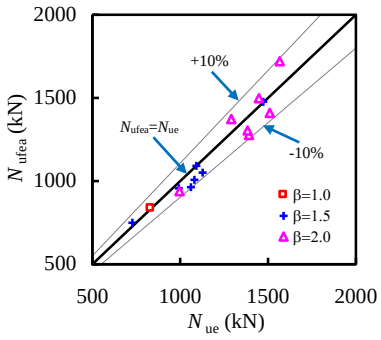

Fig. 15. Comparison between the predicted and measured bearing capacity.

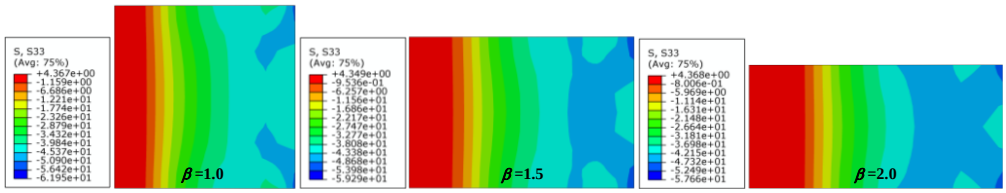

(a) Variation of β

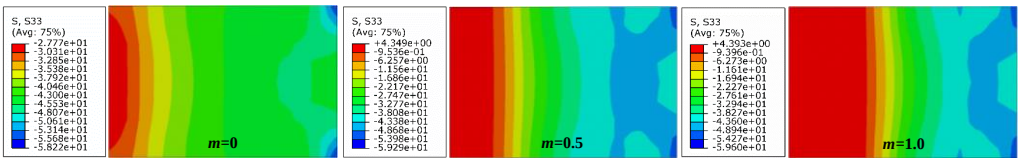

(b) Variation of m

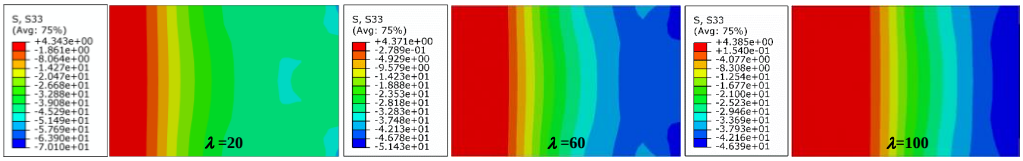

(c) Variation of λ

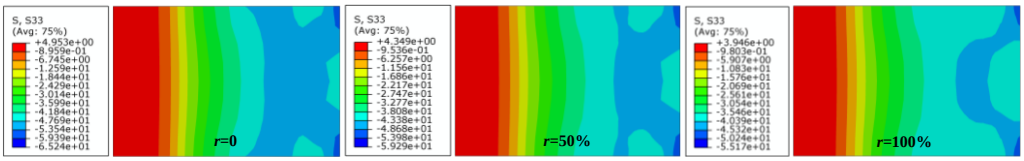

(d) Variation of r

Fig. 16. Influence of typical parameters on longitudinal stress (S33) of core RAC.

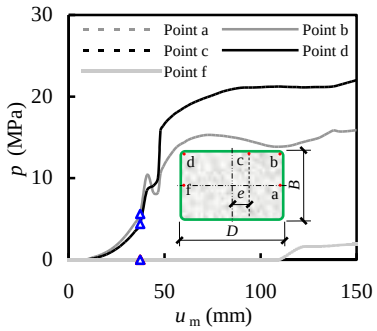

Fig. 17. Typical variation of interaction stress (p) at the mid-height section.

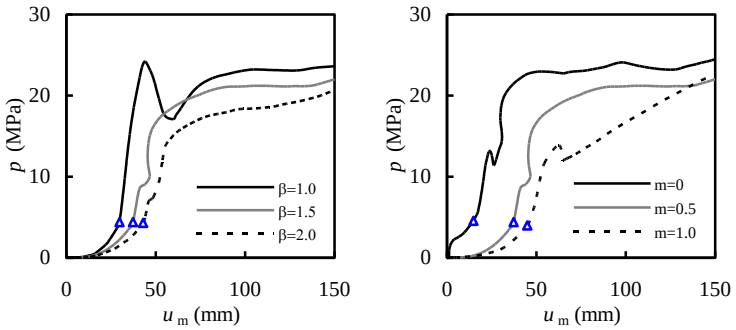

(a) Variation of β

(b) Variation of m

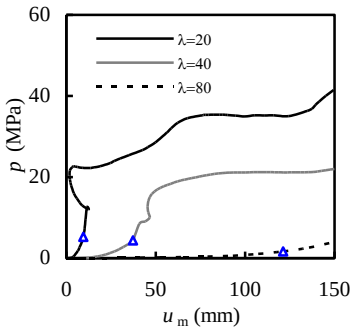

(c) Variation of λ

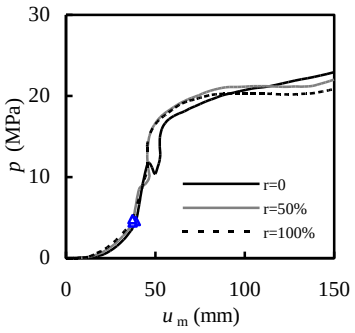

(d) Variation of r

Fig. 18. Effect of key parameters on p-u_{m} relationship at point b.

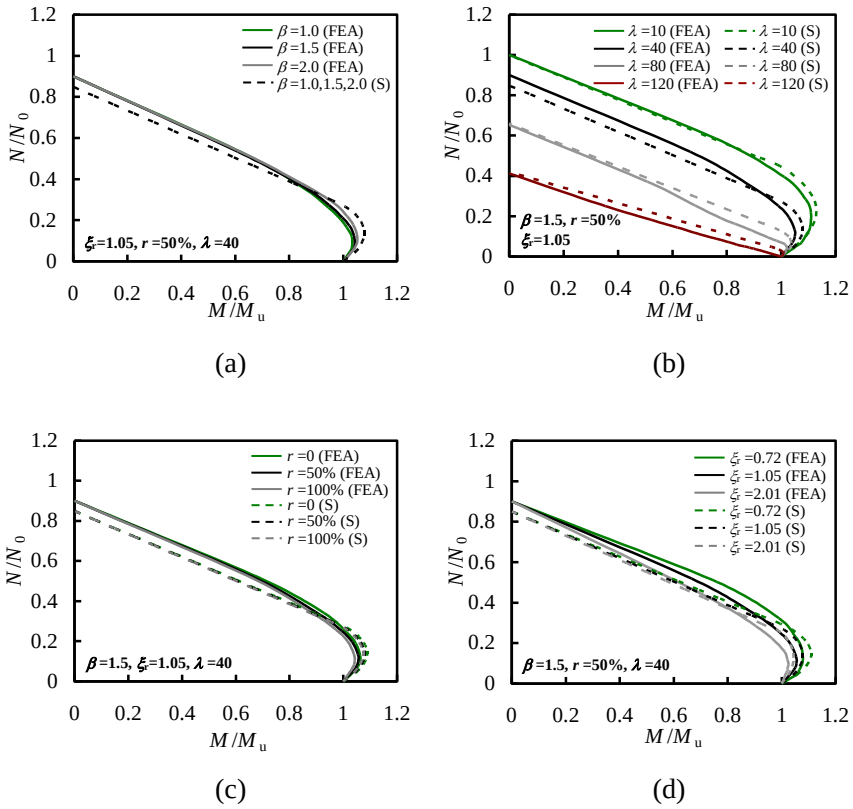

Fig. 19. Axial load ratio versus moment ratio interaction curves.

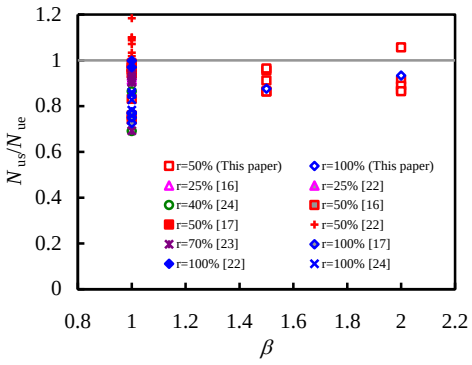

Fig. 20. Effect of β and r on N_{us}/N_{ue}.

Tables:

Table 1 Information of the specimens.

No.	Label	$D\times B\times t$ (mm×mm×mm)	H (mm)	e (mm)	β	m	λ	r (%)	N_{ue} (kN)	u_{me} (mm)	N_{ufea} (kN)	$\frac{N_{ufea}}{N_{ue}}$
1	A0.3-30-RAC1	120×120×2.7	1040	18	1.0	0.3	30	50	832.2	5.31	836.1	1.005
2	B0.3-30-RAC1	180×120×2.7	1560	27	1.5	0.3	30	50	1081.5	8.29	1007.5	0.932
3	C0.3-30-RAC1	240×120×2.7	2080	36	2.0	0.3	30	50	1391.3	10.50	1277.9	0.918
4	B0-30-RAC1	180×120×2.7	1560	0	1.5	0	30	50	1472.7	1.06	1476.5	1.003
5	B0.6-30-RAC1	180×120×2.7	1560	54	1.5	0.6	30	50	727.4	7.80	749.2	1.030
6	B0.3-20-RAC1	180×120×2.7	1040	27	1.5	0.3	20	50	1127.6	3.09	1051.1	0.932
7	B0.3-40-RAC1	180×120×2.7	2080	27	1.5	0.3	40	50	991.8	11.32	956.8	0.965
8	B0.3-30-NC	180×120×2.7	1560	27	1.5	0.3	30	0	1092.3	7.78	1091.4	0.999
9	B0.3-30-RAC2	180×120×2.7	1560	27	1.5	0.3	30	100	1061.2	8.15	963.6	0.908
10	C0-30-RAC1	240×120×2.7	2080	0	2.0	0	30	50	1566.5	0.84	1721.0	1.099
11	C0.6-30-RAC1	240×120×2.7	2080	72	2.0	0.6	30	50	996.2	11.31	939.1	0.943
12	C0.3-20-RAC1	240×120×2.7	1390	36	2.0	0.3	20	50	1509.8	4.20	1410.2	0.934
13	C0.3-36-RAC1	240×120×2.7	2495	36	2.0	0.3	36	50	1383.7	13.16	1304.3	0.943
14	C0.3-30-NC	240×120×2.7	2080	36	2.0	0.3	30	0	1448.4	10.25	1498.5	1.035
15	C0.3-30-RAC2	240×120×2.7	2080	36	2.0	0.3	30	100	1290.6	9.35	1372.5	1.063

Table 2 Mix proportion and properties of concrete.

Type	r (%)	Mix proportion (kg/m^3)						Properties			
		Cement	Sand	NCA	RCA	Water	WRA	$f_{cu,28}$ (MPa)	$f_{cu,t}$ (MPa)	E_c (GPa)	Slump height (mm)
NC	0	469	645	1098	0	195.5	3.75	57.7	68.0	38.3	230
RAC1	50	469	645	549	549	195.5	3.75	55.8	65.7	35.9	225
RAC2	100	469	645	0	1098	195.5	3.75	55.6	65.1	27.8	215